



University of  
Massachusetts  
Amherst

## Effect of Phase Composition of Tungsten Carbide on its Catalytic Activity for Toluene Hydrogenation

Item Type	Thesis (Open Access)
Authors	Rane, Aditya
DOI	<a href="https://doi.org/10.7275/24514028.0">10.7275/24514028.0</a>
Rights	Attribution 4.0 International
Download date	2026-05-16 14:07:36
Item License	<a href="http://creativecommons.org/licenses/by/4.0/">http://creativecommons.org/licenses/by/4.0/</a>
Link to Item	<a href="https://hdl.handle.net/20.500.14394/32802">https://hdl.handle.net/20.500.14394/32802</a>

**Effect of Phase Composition of Tungsten Carbide on its  
Catalytic Activity for Toluene Hydrogenation**

A Thesis Presented by

ADITYA RANE

Submitted to the Graduate School of the  
University of Massachusetts Amherst in partial fulfillment  
of the requirements for the degree of

MASTER OF SCIENCE IN CHEMICAL ENGINEERING  
September 2021

Department of Chemical Engineering

© Copyright by Aditya Rane 2021

All Rights Reserved

# Effect of Phase Composition of Tungsten Carbide on its Catalytic Activity for Toluene Hydrogenation

A Thesis Presented by

ADITYA RANE (arane@umass.edu)

Approved as to style and content by:

DocuSigned by:

*Friederike Jentoft*

6E840E1B35B5479...

Friederike Jentoft, Chair

DocuSigned by:

*Omar Abdelrahman*

6394D00F88004E7...

Omar Abdelrahman, Member

DocuSigned by:

*James Walsh*

6D25EC1BB7F5480...

James Walsh, Member

DocuSigned by:

*Michael A. Henson*

4260423F849F41B...

Michael Henson, Department Head

Department of Chemical Engineering

## ACKNOWLEDGMENTS

I have quite a few people that I want to acknowledge for their support, guidance, and counsel during this thesis. First and foremost, I would like to start by thanking my advisor Dr. Friederike Jentoft for letting me work on this beautiful thesis and for the unwavering support and guidance during the entire course of the work. It was her introduction to this project that made it an instantaneous decision for me to work on it. Her patience towards me and working to build something meaningful and at the same time being a constant source of motivation is something I will always be grateful for.

This work would not have been possible without the guidance of Dr. Rolf Jentoft who always had the perfect solutions to resolving and developing the experimental setups. I have learned so much about the physical and conceptual understanding of designing reactors, analyzing and interpretation of data, equipment trainings and so on.

I would further like to thank my committee members Dr. Omar Abdelrahman and Dr. James Walsh for their noteworthy suggestions and comments towards a better understanding of the project. The Jentoft group was always a constant source of help, fruitful discussions, and encouragement. A big thank you to Dr. Shelly Peyton for her constant efforts in the smooth functioning of the graduate program.

Finally, I would like to extend a huge gratitude to my parents who have been with me throughout this graduate program journey although not physically but have been the biggest source of mental strength and support.

## ABSTRACT

### EFFECT OF PHASE COMPOSITION OF TUNGSTEN CARBIDE ON ITS CATALYTIC ACTIVITY FOR TOLUENE HYDROGENATION

SEPTEMBER 2021

ADITYA RANE

B.E. UNIVERSITY OF MUMBAI

M.S. ChE, UNIVERSITY OF MASSACHUSETTS AMHERST

Directed by: Professor Friederike C. Jentoft

Commercially important hydrogenation reactions make use of precious noble metal catalysts which are becoming increasingly scarce, and the search for capable alternative catalysts prevails. Transition metal carbides of group IV-VI metals show similar catalytic behavior to platinum and are  $\$10^3/\text{kg}$  lower in price than the precious metal catalysts. Tungsten carbide, studied in this work, can form in different stoichiometries and phase compositions depending upon synthesis methods. Synthesis of high surface area tungsten carbide with control over its phase composition remains a challenge currently.

In this work, the novel isothermal synthesis method of tungsten carbide ( $\text{WC}$ ,  $\text{W}_2\text{C}$ ) in a  $\text{CH}_4/\text{H}_2$  carburization atmosphere with synthesis temperature and presence or absence of a silica support in the catalyst precursor ( $\text{WO}_3$ ) as process variables was investigated. The amounts of  $\text{CO}$  and  $\text{H}_2\text{O}$  formed during synthesis corresponded to the amount of oxygen in the  $\text{WO}_3$  precursor. The catalysts were further characterized by X-ray diffraction to determine phase composition and crystallite size, by scanning electron microscopy to determine morphology and by  $\text{CO}$  chemisorption to determine metallic surface area. X-ray diffraction analysis indicated the carbide catalysts to contain  $\text{W}_2\text{C}$ ,  $\text{WC}$  and metallic  $\text{W}$

phases. The use of a silica supported precursor favored the formation of a nearly phase pure, high surface area  $W_2C$  rich catalyst whereas high synthesis temperature and absence of silica precursor favored formation of a low surface area WC rich catalyst. Further, the catalysts were tested for steady state activity at a W/F (weight catalyst/toluene feed rate) of 0.20-0.30  $h^{-1}$ , addition of  $H_2$  to a total pressure of 21 bar absolute and 250 °C, and the effect of phase composition and surface area on the activity was studied. This work resulted in the successful synthesis of 4 tungsten carbide catalysts with varying phase compositions and surface areas and correlation of their compositions and surface areas with their corresponding toluene hydrogenation activities.

# TABLE OF CONTENTS

	Page
ACKNOWLEDGEMENTS.....	iv
ABSTRACT.....	v
LIST OF TABLES.....	viii
LIST OF FIGURES .....	ix
CHAPTER	
1. INTRODUCTION.....	1
2. LITERATURE REVIEW.....	6
2.1. Introduction to transition metal carbides and synthesis methods.....	6
2.2. Materials characterization.....	9
2.3. Catalysis.....	11
3. MATERIALS & RESEARCH METHODOLOGY.....	13
3.1 Development of isothermal synthesis method.....	13
3.2 X-ray diffraction measurement and analysis.....	17
3.3 Carbon monoxide chemisorption.....	18
3.4 High pressure toluene hydrogenation.....	19
4. RESULTS & DISCUSSIONS .....	21
4.1 Isothermal tungsten carbide syntheses .....	21
4.2 Characterization of the catalyst samples .....	27
4.2.1 Phase composition analysis.....	28
4.2.2 Crystallite size analysis.....	33
4.2.3 Scanning electron microscopy(SEM) imaging.....	34

4.3 Surface area measurements using CO chemisorption .....	37
4.4 Toluene hydrogenation activity .....	44
5.SUMMARY AND CONCLUSION .....	47
6. FUTURE WORK.....	51
APPENDICES.....	53
REFERENCES.....	61

## LIST OF TABLES

<b>Table</b>	<b>Page</b>
Table 1: Operating parameters for isothermal syntheses of tungsten carbide .....	21
Table 2: Average amounts of H <sub>2</sub> O and CO produced per mmol WO <sub>3</sub> for the isothermal syntheses .....	26
Table 3: Phases and space groups used for XRD analysis.....	27
Table 4: Crystalline domain sizes of WC and W <sub>2</sub> C particles .....	33
Table 5: Sample CO chemisorption calculation template.....	58
Table 6: Safety limits of gases used.....	59

## LIST OF EQUATIONS

<b>Scheme</b>	<b>Page</b>
Scheme 1: Reaction stoichiometry for toluene hydrogenation .....	5
Scheme 2: Proposed reduction-carburization reaction pathway .....	8
Scheme 3: Stability order of the different phases formed in the tungsten carbide system .....	10
Scheme 4: Stoichiometric reaction for formation of $W_2C$ using $WO_3$ precursor .....	22
Scheme 5: Stoichiometric reaction for formation of $WC$ using $WO_3$ precursor .....	22
Scheme 6: Stoichiometric reaction for formation of $W$ using $WO_3$ precursor .....	22

## LIST OF FIGURES

Figure	Page
Figure 1: Crystal structures of $\alpha$ -WC and $\beta$ -W <sub>2</sub> C phases.....	2
Figure 2: Group IV-VII transition metals and their stable carbides and nitrides.....	7
Figure 3: Schematic of the timeline of a temperature-programmed reduction carburization pathway and an isothermal synthesis pathway for tungsten carbide synthesis .....	9
Figure 4: Toluene hydrogenation reaction pathways.....	12
Figure 5: Packed bed reactor system with loaded precursor material .....	14
Figure 6: Reactor manifold assembly .....	15
Figure 7: Temperature ramp timeline of the isothermal tungsten carbide synthesis protocol.....	16
Figure 8: Reference X-ray powder diffraction intensities of metallic tungsten and its carbide phases from ICDD database (W: 00-004-0806, W <sub>2</sub> C: 00-035-0776, WC: 00-025-1047) .....	18
Figure 9: Reduction signals at 700 °C isothermal period using a 50 mg WO <sub>3</sub> /SiO <sub>2</sub> precursor in a CH <sub>4</sub> /H <sub>2</sub> flow .....	23
Figure 10: Reduction signals at 750 °C isothermal period using a 50 mg WO <sub>3</sub> /SiO <sub>2</sub> precursor in a CH <sub>4</sub> /H <sub>2</sub> flow .....	23
Figure 11: Reduction signals at 700 °C isothermal period using a 30.5 mg bulk WO <sub>3</sub> precursor in a CH <sub>4</sub> /H <sub>2</sub> flow .....	24
Figure 12: Reduction carburization signals at 750 °C isothermal period using 30 mg bulk WO <sub>3</sub> precursor in a CH <sub>4</sub> /H <sub>2</sub> flow .....	25
Figure 13: Oxygen balance average for all 4 types of syntheses .....	26
Figure 14: Measured diffractograms for 4 syntheses with their stacked pattern references .....	28
Figure 15: XRD phase fitting of 700 °C synthesis using WO <sub>3</sub> /SiO <sub>2</sub> precursor .....	29
Figure 16: XRD pattern fitting of a 700 °C synthesis using WO <sub>3</sub> bulk precursor .....	30

Figure 17: XRD pattern fitting of a 750 °C synthesis using WO <sub>3</sub> /SiO <sub>2</sub> precursor .....	31
Figure 18: XRD pattern fitting of a 750 °C synthesis using WO <sub>3</sub> precursor .....	32
Figure 19: Single crystal morphology of a tungsten carbide catalyst .....	34
Figure 20: Topological features of a tungsten carbide surface .....	35
Figure 21: SEM image of a tungsten carbide catalyst synthesized at 750 °C using bulk WO <sub>3</sub> .....	36
Figure 22: Temperature timeline for a CO chemisorption experiment.....	37
Figure 23: CO chemisorption for a 700 °C WO <sub>3</sub> /SiO <sub>2</sub> precursor synthesis .....	38
Figure 24: Cumulative CO adsorption curve for a catalyst synthesized at 700 °C using WO <sub>3</sub> /SiO <sub>2</sub> precursor .....	39
Figure 25: CO chemisorption for a 700 °C bulk WO <sub>3</sub> precursor synthesis .....	39
Figure 26: Cumulative CO adsorption curve for a catalyst synthesized at 700 °C using a bulk WO <sub>3</sub> precursor.....	40
Figure 27: CO chemisorption for a 750 °C WO <sub>3</sub> /SiO <sub>2</sub> precursor synthesis .....	41
Figure 28: Cumulative CO adsorption curve for a catalyst synthesized at 750 °C using a WO <sub>3</sub> /SiO <sub>2</sub> precursor .....	41
Figure 29: CO chemisorption pulses for a sample synthesized at 750 °C bulk WO <sub>3</sub> precursor.....	42
Figure 30: Cumulative CO adsorption curve for a catalyst synthesized at 750 °C using a WO <sub>3</sub> precursor .....	42
Figure 31: CO adsorbed amounts for the 4 different catalyst syntheses conditions.....	43
Figure 32: Toluene hydrogenation activity of the 4 tungsten carbide catalysts .....	44
Figure 33: Site time yield for the catalyst materials .....	45
Figure 34: Loss of activity of a fresh and chemisorption performed catalyst .....	46
Figure 35: Phase composition summary based on catalyst synthesis conditions .....	48

Figure 36: CO adsorption capacity based on the catalyst synthesis conditions.....	49
Figure 37: Effect of increasing W <sub>2</sub> C content on surface area.....	50
Figure 38: Moles H <sub>2</sub> O injection pulses vs their respective peak areas of the ion current signals using mass spectrometry.....	53
Figure 39: Moles CO pulses vs their respective peak areas of the ion current signals using mass spectrometry.....	54
Figure 40: Uncertain evidence for quantitative interpretation of CH <sub>4</sub> , H <sub>2</sub> consumption or CO <sub>2</sub> formation traces during synthesis period. ....	55
Figure 41: Flat line nature of m/z 18 H <sub>2</sub> O signal during carbide synthesis.....	56
Figure 42: 6 port GC valve configuration for CO chemisorption.....	56
Figure 43: Appearance of silica background at 20-25° 2θ.....	57

# CHAPTER 1

## INTRODUCTION

Interstitial carbides of group IV-VI transition metals are compounds that are formed by insertion of carbon atoms in the interstitial sites of the transition metal. This addition of carbon alters the structural and electronic properties of the parent metal resulting in interesting catalytic behavior similar to highly active noble metals like platinum and palladium.<sup>1,2</sup> Carbides of the transition metals ( $\text{Mo}_2\text{C}$ ,  $\text{WC}$ ,  $\text{TiC}$ ) have been explored as potential replacement catalysts for the noble metals like platinum which are most employed for a variety of catalytic reactions including hydrogenation, hydrogenolysis and hydrodeoxygenation.<sup>3,4</sup>

From an economical perspective, the major benefit with the metal carbide catalysts are the material costs for the tungsten and molybdenum metals being 3 orders of magnitude lower (\$10/kg) than platinum or gold (\$10<sup>4</sup>/kg) whereas their abundance in the earth's crust is 2 orders of magnitude higher compared to the precious noble metals.<sup>5</sup> They also have the advantage of being resistant to sulfur poisoning during conversion of heavy aromatics to fuels.<sup>6</sup>

The limiting aspect of the carbide structures is their surface area which limits their application in comparison to high surface area noble metal catalysts. Industrial synthesis of carbide materials involves extremely high temperatures (1200-1600 °C), and the resulting carbides have low specific surface area  $S_g$  and thus are unsuitable as catalysts.<sup>7</sup>

Another complexity arises from the existence of polymorphs for some of the transition metal carbides. Tungsten carbide, the subject of this thesis, has been shown to form in two different stoichiometries and crystal structures (Fig.1),  $\beta\text{-W}_2\text{C}$  which is a metastable phase, and forms at lower temperatures and  $\alpha\text{-WC}$  which is the thermodynamically favored phase. The  $\alpha\text{-WC}$  structure

exists in a simple hexagonal lattice structure whereas the  $\beta$ -W<sub>2</sub>C is a hexagonal close packed arrangement.<sup>8</sup>

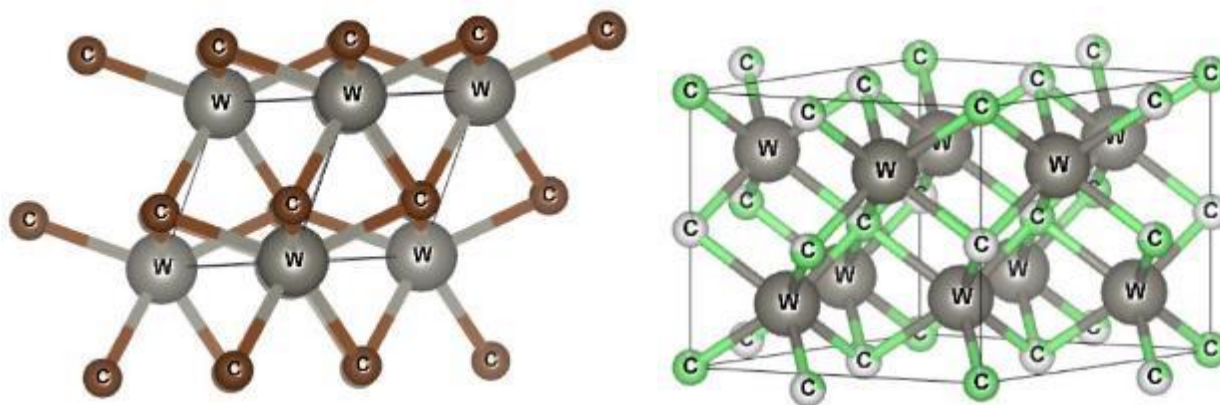


**Figure 1: Crystal structures of  $\alpha$ -WC and  $\beta$ -W<sub>2</sub>C phases**

Significant research has been done towards the catalytic application standpoint for the carbides, but less focus has been subjected to the synthesis and influence of synthesis parameters on the final phase composition of the carbide and the resulting surface area of the catalysts.<sup>9-11</sup> For their use in catalytic applications, the control of phase composition and a higher specific surface area and lower synthesis temperatures are the important factors.<sup>11-13</sup> There is extremely limited information on how to obtain these catalysts with a control over their phase composition and higher surface areas. Thus, one of the major objectives of this work was to develop a method which can, in hindsight provide a better control over a certain phase for the tungsten carbide system and establish how the resulting phase composition in turn affects the catalytic activity for toluene hydrogenation test reaction.<sup>14,15</sup>

The syntheses conditions influence the final phase composition of the carbide. The investigation of the influence of synthesis conditions and optimization have been carried out in an empirical manner. A temperature-programmed reduction carburization method for the synthesis of tungsten carbide using tungsten oxide as precursors is the most employed synthesis pathway.<sup>11</sup> In

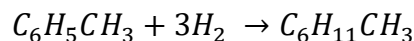
this work, we employ an isothermal reduction-carburization method for the synthesis of these carbide catalysts. The isothermal synthesis employed in this project has not been studied extensively, and very few works are available on how the synthesis compares to the extensively investigated temperature-programmed reduction-carburization (TPRC) method.<sup>11,15</sup> The motivation for implementation of the isothermal method is twofold: a) Understanding the phase composition preference based on the synthesis conditions and b) Sintering of particles is a major reason for catalyst deactivation and it is avoided at lower synthesis temperatures.<sup>16</sup> The synthesis is governed by the reduction rates of surface and bulk phases, carbon activation and migration on the surface and into the bulk. The stability of carbide or metal phase and thus the overall method need to be well refined for understanding these governing factors.<sup>11,13</sup> The reduction proceeds differently with the isothermal method in that the pre-reduction of precursor which takes place in a TPRC synthesis method is avoided, and the reduction only begins at isothermal synthesis temperature.<sup>15</sup> The effect of the synthesis conditions on the resulting phase composition and surface area of the catalysts is fundamental to the optimization of the tungsten carbide catalysts.<sup>17,18</sup>

The catalyst precursor choice was also fundamental to the final phase composition obtained after the carbide synthesis. A silica-supported tungsten trioxide was found to stabilize and increase the  $W_2C$  phase composition and resulted in increased activity for butyraldehyde hydrogenation. In this work, we intended to test whether the trend found for butyraldehyde hydrogenation also pertains to the chosen test reaction for this work.<sup>15</sup>

Characterization of these materials is based on X-ray diffraction that provides information on the crystal structure of the metallic carbides since they can exist in different stoichiometries and the phase composition of the material. Whole powder pattern fitting is employed to obtain the final phase composition and crystallite sizes of each identified phase. In terms of metallic carbides,

scanning electron microscopy is also performed on the materials to elucidate the structural/surface features of these materials. Backscattered electron images that depend on the atomic number of the elements can potentially describe the distribution of the parent metal and carbon atoms.<sup>19</sup> Since high surface area is a fundamental requirement for catalysis, one of the objectives of this work involved synthesis of tungsten carbide materials with a high surface area while also having control over the phase composition. In essence, surface area of a catalyst is indicative of the number of catalytically active sites present on the catalyst surface. In terms of reaction kinetics, it aids in characterizing the catalysts by the intrinsic activity of each site by correlating activity to the number of sites or as turnover frequency. CO chemisorption is a characteristic surface area determination technique to measure the surface area of a catalyst in terms of CO uptake in moles per mole of catalyst.<sup>20,21</sup>

Some hydrogenation reactions exhibit a structure sensitive relationship towards a catalyst structure. Structure sensitivity of a reaction can be described as the dependence of the rate of reaction on the surface anisotropy that can be further divided into either the different crystal directions or the particle size of crystals.<sup>22</sup> Since tungsten carbide forms in two phase structures (WC, W<sub>2</sub>C), one of the goals of the thesis was to understand how the catalysts rich in either of these phases correlated with the catalytic activity. Tungsten carbide and molybdenum carbide have similarly been well investigated for their activity in catalytic hydrogenation reactions which make use of the expensive noble metal catalysts for commercial as well as industrial purposes.<sup>2,4,18</sup> Since we are interested in the structure activity relationships of the tungsten carbide catalysts, a test reaction was needed, and we chose toluene hydrogenation reaction with a ring hydrogenation mechanism that leads to methylcyclohexane as a sole product. The reaction stoichiometry can be described as:



**Scheme 1: Reaction stoichiometry for toluene hydrogenation**<sup>23</sup>

The rationale for this catalytic test is that toluene serves as a platform molecule for industrially relevant reactions. Catalytic ring hydrogenation has been found to be structure sensitive meaning the reaction rates are dependent on several surface aspects including but not limited to the particle size of the metallic nanoparticles.<sup>24</sup> Toluene is also a model molecule for heavy oil and polycyclic aromatic chemistries. On the other hand, hydrogen has gained interest as being an alternative energy source because of its high energy density, and the need for efficient hydrogen carriers for storage of hydrogen and an organic hydride couple of toluene/methylcyclohexane have been under focus. The hydrogen storage capacity for the toluene/methylcyclohexane couple (6.2 wt%) is much higher than those of the commercially used H<sub>2</sub> storage alloys that are around 1-2 wt%.<sup>25</sup>

The structure of this project was designed such that we delve into the relevant literature and some preliminary work to formulate a research plan. This involved modifications to the existing experimental setups and establishing experimental protocols that helped us achieve the research goals. The overarching goal of this project was to establish a structure-activity relationship of tungsten carbide catalysts for toluene hydrogenation reaction, and a phase pure carbide catalyst is essential to elucidate this structure-activity phenomenon.

## CHAPTER 2

### LITERATURE REVIEW

#### 2.1. Introduction to transition metal carbides and synthesis methods

Transition metals have an exceptional ability to form compounds with lighter elements like oxygen, nitrogen, and carbon. These metals that belong to groups III-XII in the periodic table are notably interesting and widely researched for their diverse set of properties, features and chemistry involved with them. They are basically termed as transition elements since the d sublevel is incompletely filled while the s sublevel is filled before the d sublevel.<sup>8,26</sup> The metal carbide thus formed has a characteristic property set derived from properties of three types of materials. These structures show extreme hardness which is a characteristic of covalent solids; high melting temperatures which are exhibited by ionic crystals whilst retaining the electronic and thermal properties of parent transition metals. The structures of such compounds are diverse in their properties, and their applications depend upon the parent metal and its interaction with the interstitial carbon atoms. In terms of geometry, the stability of these structures is predicted by Hagg's rule. It states that the ratio of the nonmetallic to the metallic radii should lie between 0.41-0.59.<sup>27</sup>

Group IV-VI transition metals are especially the elements that can form stable compounds with carbon in varying stoichiometries. Group III and VII-XII metals do not form stable carbides or nitrides except for iron.<sup>28</sup> Major transition metals and their carbide/nitride stoichiometries are described in Figure 2.

IVB	VB	VIB	VIIB
Ti*	V	Cr	Mn
Zr	Nb	Mo	Tc
Hf	Ta	W	Re

<span style="display:inline-block; width:15px; height:15px; background-color:lightgreen;"></span> MC/MN	<span style="display:inline-block; width:15px; height:15px; background-color:lightblue;"></span> $M_3C_2/M_3N_2$
<span style="display:inline-block; width:15px; height:15px; background-color:yellow;"></span> $MC_{1-x}/MN_{1-x}$	<span style="display:inline-block; width:15px; height:15px; background-color:purple;"></span> $M_2C/M_2N$
<span style="display:inline-block; width:15px; height:15px; background-color:lightpink;"></span> No stable carbide/nitride	

**Figure 2: Group IV-VII transition metals and their stable carbides and nitrides<sup>28</sup>**

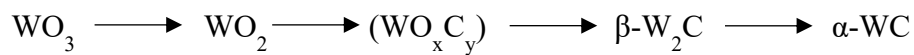
Figure reproduced under creative commons license CC-BY 4.0 from Zhong Y., Xia X., Shi F., Zhan J., Tu J., Fan H. J. (2016). (Ref.28)

This leads to a noble metal like behavior of carbides and nitrides of group VI early transition metals such as molybdenum and tungsten, and thus they have shown remarkable promise in catalytic reactions ranging from hydrogenation and isomerization to hydrodeoxygenations.<sup>2,14,29</sup> Even though the physical and electronic properties of the transition metal carbides and noble metals are similar, the observed activity and stability of the carbides might be affected by low surface areas and the contamination of surfaces with excess (polymeric) carbon or oxygen.<sup>30,31</sup> The similarity to the noble metals lies in the change in the electron distribution in tungsten with addition of carbon resulting in lower reactivity of tungsten towards oxygen by adding valence electrons to the metal orbital. The objective thus is careful control of the amount of carbon addition which can provide optimum results.<sup>9,13</sup>

Oyama described a temperature-programmed synthesis method of tungsten carbides with high specific surface areas and existence of both the phases  $\alpha$ -WC and  $\beta$ -W<sub>2</sub>C.<sup>12</sup> The influence of

the concentration of CH<sub>4</sub> and H<sub>2</sub> on the reduction carburization kinetics of the WO<sub>3</sub> precursor was investigated. Varying the amount of CH<sub>4</sub>:H<sub>2</sub> mixture influenced the phase change from β-W<sub>2</sub>C to α-WC in that the partial pressure dependence ( $P_{\text{CH}_4}/P_{\text{H}_2}$ ) controlled the rate of carbon deposition on the surface of the solid. The β-W<sub>2</sub>C phase was only observed for a ( $P_{\text{CH}_4}/P_{\text{H}_2}$ )=1 whereas for ( $P_{\text{CH}_4}/P_{\text{H}_2}$ )>1, the carbon diffusion into β-W<sub>2</sub>C led to faster formation rates of α-WC but also led to deposition of polymeric carbon on the surface.<sup>11,32</sup>

The reduction carburization process under two different hydrocarbon gas mixtures (20% CH<sub>4</sub>/H<sub>2</sub> and 10% C<sub>2</sub>H<sub>6</sub>/H<sub>2</sub>) also showed an influence on the final structure and catalytic performance of the carbide materials. The use of 10% C<sub>2</sub>H<sub>6</sub>/H<sub>2</sub> resulted in carbides with higher surface areas since ethane was a more active carbon source and the reduction could take place at lower temperature (600 °C) as compared to 20% CH<sub>4</sub>/H<sub>2</sub> (700 °C), but the use of ethane also led to polymeric carbon deposition which resulted in lowering of the surface areas. A potential reduction-carburization pathway was developed as per the phases observed during a temperature-programmed reduction-carburization synthesis using in-situ X-ray diffraction to observe phase transitions. The presence of an oxycarbide phase (WO<sub>x</sub>C<sub>y</sub>) was observed only in carburizations using a CH<sub>4</sub>-H<sub>2</sub> mixture.<sup>13,33</sup>



**Scheme 2: Proposed reduction-carburization reaction pathway<sup>13</sup>**

The difference in the actual processes of a temperature-programmed reduction carburization and an isothermal synthesis (as described in Figure 3) was studied, and it was found that the isothermal synthesis can produce a W<sub>2</sub>C rich carbide phase composition as opposed to the temperature-programmed reduction carburization that exhibited a preference to all three phases.

The control over the  $W_2C$  phase for a carbide surface was shown to be highly dependent on temperature, and to some extent the silica stabilizer support added to the precursor material controlled excess carbon deposition on the catalyst surface.<sup>15</sup>

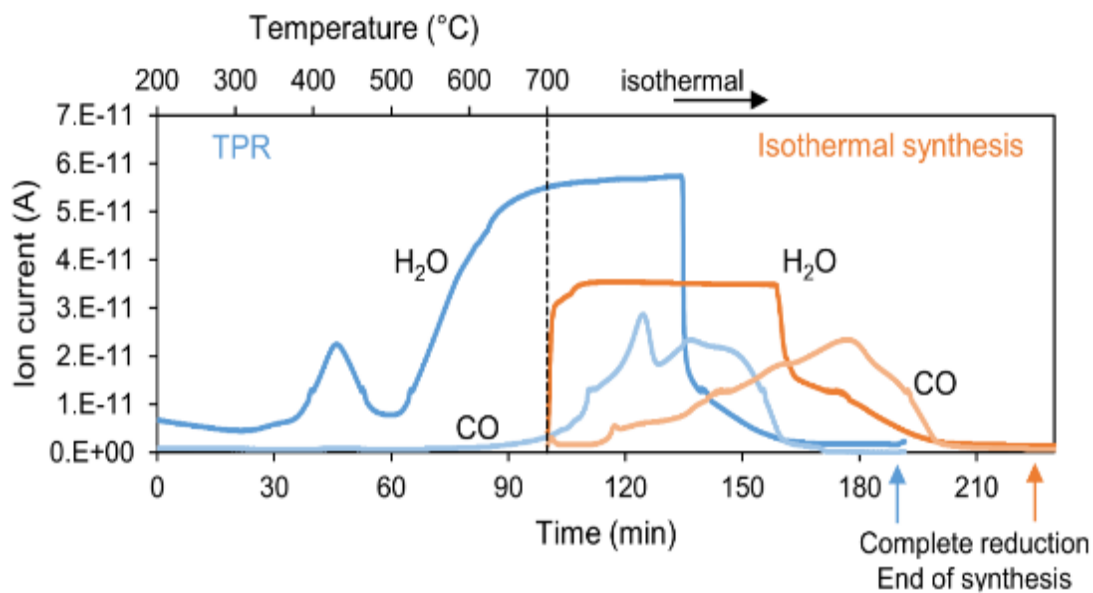
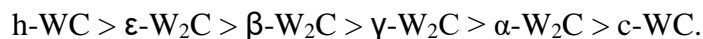


**Figure 3: Schematic of the timeline of a temperature-programmed reduction carburization pathway and an isothermal synthesis pathway for tungsten carbide synthesis**<sup>15</sup>

## 2.2 Materials characterization:

Tungsten carbide as described before, exists in two phase systems WC and  $W_2C$ . The  $W_2C$ , known as tungsten semi carbide, is a metastable phase formed during the synthesis which exists in a hexagonal close packed geometry and forms 4 different structural polymorphs ( $\alpha$ ,  $\beta$ ,  $\gamma$  and  $\epsilon$ - $W_2C$ ). The WC, also known as tungsten monocarbide is a simple hexagonal or cubic structure (h-WC or c-WC) with a space group of  $P\bar{6}m2$ .<sup>34-37</sup> The  $W_2C$  phase exists in 4 different space groups ( $P\bar{6}_3/mmc$ ,  $Pbcn$ ,  $P\bar{3}m1$  and  $P\bar{3}1m$ ) based on its 4 polymorphic structures, which have similar structures and hence are difficult to distinguish with X-ray diffraction measurements. This is also

in part because these structures have the same tungsten lattice whereas the scattering factor based on carbon is considerably lower. The order of stabilities of the monocarbides and semi carbides based on their formation energies was studied which showed three forms of the carbide system to be most stable ( $E_{\text{form}} < 0$ ). These three phases ( $\text{h-WC}$ ,  $\epsilon\text{-W}_2\text{C}$ ,  $\beta\text{-W}_2\text{C}$ ) and the rest of the phases in increasing order of their formation energies are arranged in the following order:



**Scheme 3: Stability order of the different phases formed in the tungsten carbide system**<sup>34</sup>

The crystallite sizes reported across several works vary although the WC crystals usually are larger in their crystalline domain sizes than  $\text{W}_2\text{C}$ . Some of the average reported sizes of the WC crystals are  $> 9$  nm whereas for the  $\text{W}_2\text{C}$  structure, these sizes are in the range  $> 6$  nm.<sup>37</sup>

The carbide catalysts exhibit a wide range of surface areas depending on the synthesis conditions and catalyst supports, and optimization of syntheses parameters has been found to be essential to obtain high surface area carbide catalysts. The surface area of the transition metal carbides has been reported by both  $\text{N}_2$  physisorption BET area analysis as well as CO chemisorption measurements.  $\text{N}_2$  physisorption which is performed at liquid  $\text{N}_2$  temperatures probes the total surface area of a material and is independent of the chemical nature. CO, on the other hand at milder temperature conditions (30/40 °C) selectively adsorbs on the metallic surface. The reported BET surface areas for  $\text{Mo}_2\text{C}$  and  $\text{W}_2\text{C}$  catalysts synthesized with the same carburization mixture and starting precursors and measured after passivation in 1 vol%  $\text{O}_2/\text{He}$  were 33 and 13  $\text{m}^2/\text{g}$ . The CO uptake measured in situ on a fresh catalyst was higher for  $\text{W}_2\text{C}$  (5.4  $\mu\text{mol CO}/\text{m}^2$  catalyst) than for  $\text{Mo}_2\text{C}$  (4.3  $\mu\text{mol CO}/\text{m}^2$  catalyst).<sup>38</sup> The surface area of the fresh carbides and those after passivation in an  $\text{O}_2/\text{He}$  mixture were compared, and it was found that both the carbide samples lost substantial area after the passivation process. The surface areas of the fresh

carbides were reported to be 58 and 35 m<sup>2</sup>/g which were reduced to 43 and 23 m<sup>2</sup>/g for Mo<sub>2</sub>C and W<sub>2</sub>C respectively.<sup>14</sup> The effect of carburization gas mixtures on the final carbide structure was also investigated, and the surface area of tungsten carbide using C<sub>2</sub>H<sub>6</sub>/H<sub>2</sub> mixture was found to be higher than using CH<sub>4</sub>/H<sub>2</sub> as the carburization mixture.<sup>8,13</sup> Recent developments in trying to obtain the transition metal carbides with higher surface area and stability are focused on using carbon supports in the form of carbon nanotubes. The resultant carbide surface area was improved using activated carbon as the support material for the carbide catalysts.<sup>29</sup>

### 2.3 Catalysis

Levy and Boudart in their pioneer work showed the similarities between the transition metal carbides (TMC's) and noble metals for similar catalytic reactions and the remarkable chemistry of these transition metal carbides. They found excellent catalytic behavior of tungsten carbide in the isomerization of neo pentane which was only made possible by noble metal catalysts prior to carbide discovery.<sup>2</sup> These transition metal carbides especially tungsten carbide was also found to be highly active for electrocatalytic reactions mainly the hydrogen evolution reaction and electrolyte fuel cell applications.<sup>39-41</sup>

Hydrogenation reactions using noble metals have been explored extensively since these reactions are commercially and industrially significant in producing specialty chemicals and transforming important organic compounds like benzene and ethylene into cyclohexanes and saturated hydrocarbons. Homogenous or heterogenous catalysts, are both employed for these reactions but in recent time, most of the focus has been on heterogenous catalysts including noble metals like platinum or palladium and transition metals involving W, Mo, Ni etc.<sup>42</sup> Reactions involving C-H bond activation, H<sub>2</sub> transfer and ring hydrogenation are favorable on transition metal carbide

surfaces. Structure sensitivity of catalytic reactions is an interesting phenomenon which describes how one catalytic reaction has the tendency to react differently on different catalytic surfaces of the same material. The factors influencing this phenomenon include particle sizes and structural features of metal atoms on catalyst surfaces.<sup>43,44</sup>

Toluene hydrogenation is explored both on noble metals and tungsten and molybdenum based catalysts, and the reaction has different possible pathways depending on the type of catalyst, and reaction conditions.<sup>45,46</sup> At mild reaction temperatures, only ring hydrogenation takes place, and no other reactions are observed. A proposed model of the reaction network based on toluene is described in Figure 4. The turnover rates of benzene and toluene hydrogenation were found to change with change in nanoparticle size of a platinum catalyst.<sup>47</sup>

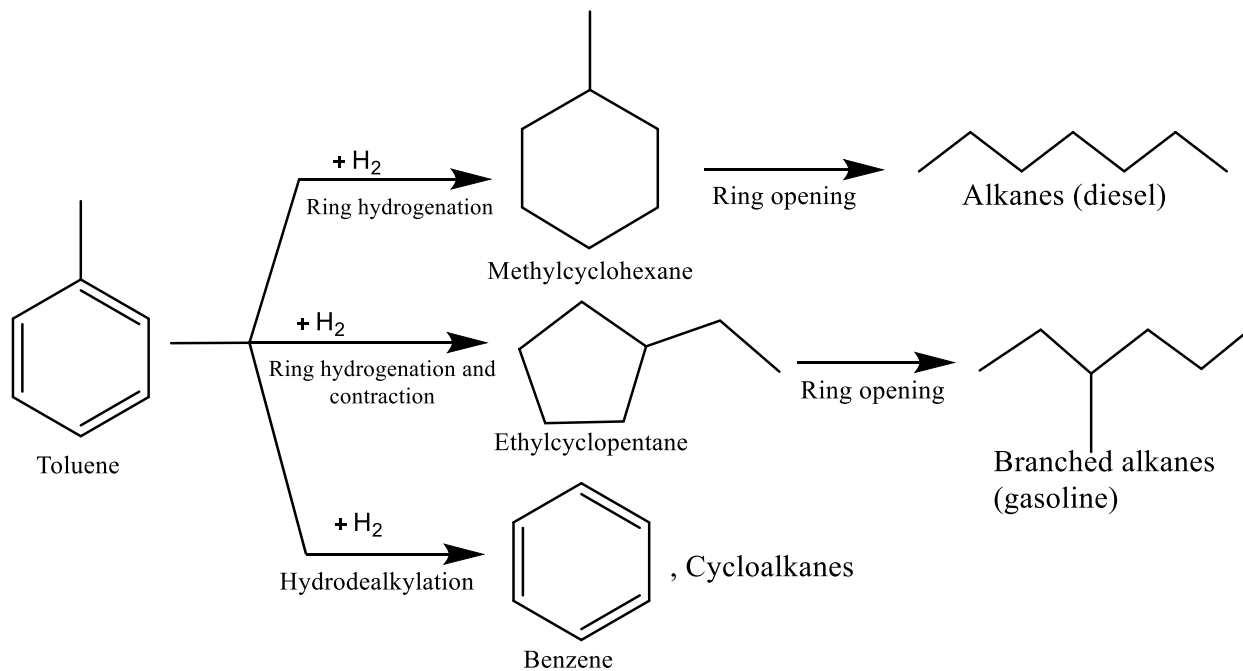


**Figure 4: Toluene hydrogenation reaction pathways<sup>45,46,48</sup>**

The reaction order for toluene hydrogenation to methylcyclohexane over molybdenum carbide catalyst was found to be 1 with respect to hydrogen and 0 in case of toluene for the investigated kinetic studies using these catalysts.<sup>48</sup>

## CHAPTER 3

### RESEARCH METHODOLOGY

#### 3.1 Development of the isothermal pathway of tungsten carbide synthesis.

The isothermal synthesis of tungsten carbide was done using a stainless-steel reactor tube (SS 316) with an outer diameter of 0.25" and a length of 17". The reactor is heated by a tubular furnace. The reactor is attached to an assembly of gas flow lines using Swagelok fittings. The same reactor was used for CO chemisorption and high-pressure toluene hydrogenation experiments.

The precursor material for the isothermal synthesis was a silica-stabilized tungsten trioxide powder ( $\text{WO}_3/\text{SiO}_2$ ) obtained from TUM Munich. The precursor for the remaining set of syntheses was a commercial/bulk  $\text{WO}_3$  obtained from Sigma Aldrich. The reactor tube is set up in a packed bed form with the precursor material loaded in between two pieces of quartz wool to hold the precursor in place. This precursor assembly is fixated in around the central zone of the reactor, and an external thermocouple temperature control element touches this zone at the outside wall of the reactor furnace to ensure the temperature is precisely controlled and monitored using an Omega CN-444 temperature controller device.

The temperature ramp is also setup using the controller with the desired temperature ramp rates.

A schematic of the packed bed reactor and flow system is described in Figure 5.

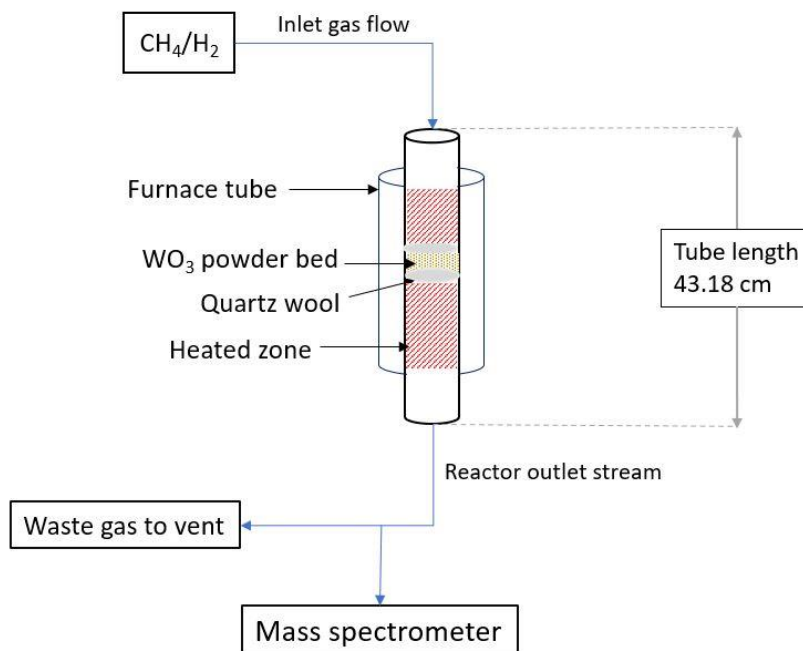


**Figure 5: Packed bed reactor system with loaded precursor material**

Adequate amount of quartz wool is loaded to hold the precursor powder and to avoid any material falling through the reactor tube. This portion of the precursor is supported using a 1/8" tube inserted through the bottom of the reactor tube all the way to the center where the precursor bed sits. This ensures the central arrangement of the bed inside the reactor where the external thermocouple contacts the region and ensures accurate temperature control during the synthesis process.

The reactor manifold setup used in this work is shown and described in Figure 6.

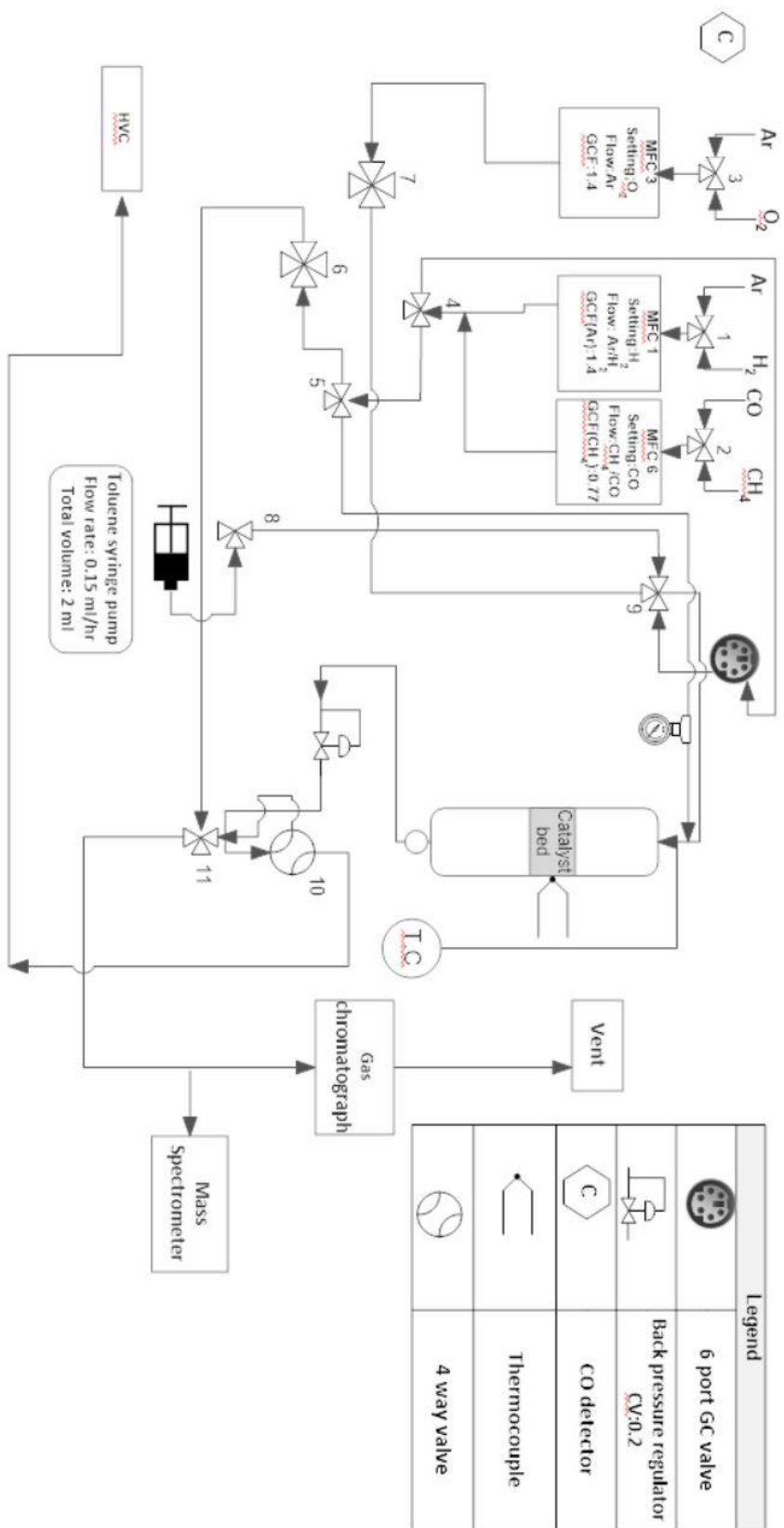


**Figure 6: Reactor manifold assembly**

The manifold setup describes the gas flow system using mass flow controllers as well as the individual components required for the synthesis and toluene hydrogenation tests.

The synthesis process was monitored and quantified using a Pfeiffer Omnistar GSD320 Mass Spectrometer. Additionally, the lines downstream of the reactor were heated adequately to avoid any condensation occurring during the synthesis. A temperature timeline profile of the isothermal synthesis method is described in Figure 7. Additionally, the mass spectrometer capillary line connected to reactor outlet was insulated since that was found to be one of the factors leading to a condensation profile of H<sub>2</sub>O signal during the synthesis, which is further described in Figure 41 in Appendix I. Calibration experiments listed in Appendix I, using pulses of both H<sub>2</sub>O and CO of known amount of molar volume and 4 different concentrations were performed to further quantify the reduction signals occurring during the actual synthesis.

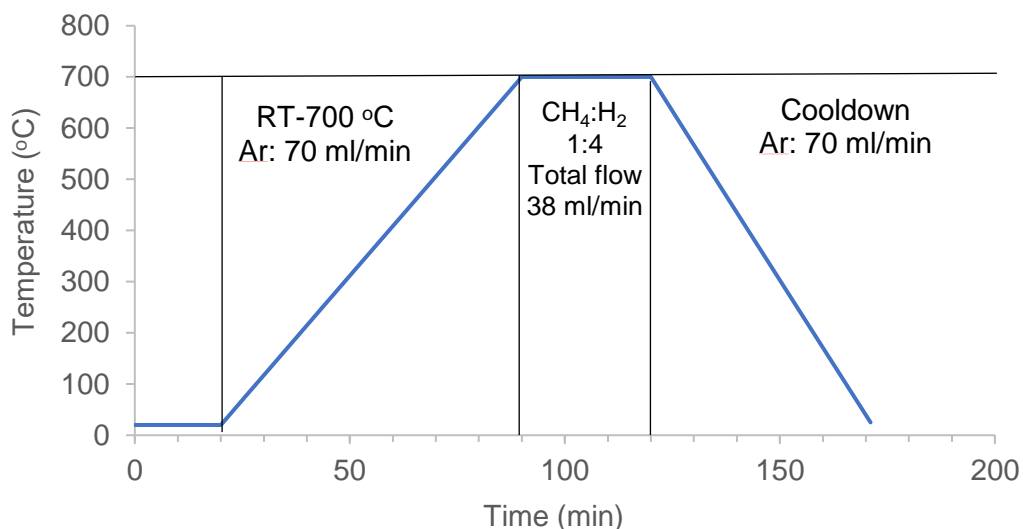


**Figure 7: Temperature ramp timeline of the isothermal tungsten carbide synthesis protocol**

### 3.2 X-ray diffraction measurement and analysis:

Characterization of the synthesized catalysts was the next pivotal step in determining the crystal structure, crystal domain size, and the composition of these catalyst materials. X-ray diffraction is a widely used technique in identification and determination of crystallite structures, size of crystalline domains and composition of a material. Thus, our synthesized materials were characterized using X-ray diffraction. The X-ray diffraction measurements were performed using a Rigaku Smartlab SE X-ray Diffraction System equipped with a Cu K $\alpha$  anode X-ray source. A scanning rate of 2 ° $\theta$ /min and a step size of 0.02° were used for the diffractogram measurement. A zero-background sample holder was used to place and mount the sample on the sample holder platform of the XRD equipment. Whole powder pattern fitting was employed to fit the measured diffractograms using Rigaku Smartlab software. Crystallite size analysis was also performed using the same software package using the Halder-Wagner method for size and strain analysis to obtain information about the crystallite sizes of various phases of tungsten carbide. The expected phases and their XRD patterns are shown in Figure 8 with the reference patterns for the three phases. For instance, the peak at 50 °2 $\theta$  for WC is a good distinction between WC and other two phases<sup>49-51</sup>.

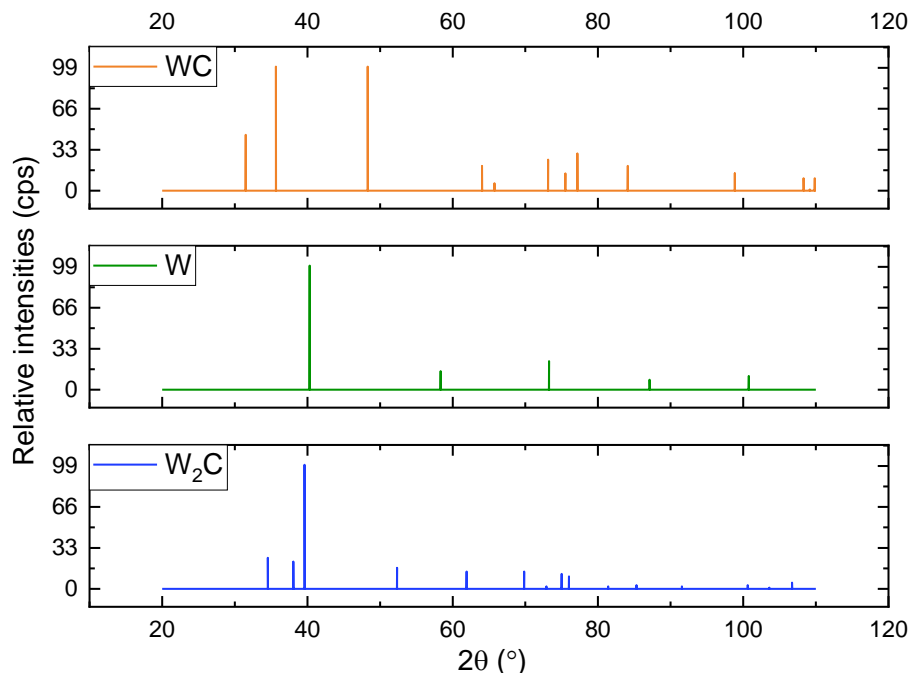


**Figure 8: Reference X-ray powder diffraction intensities of metallic tungsten and its carbide phases from ICDD database (W: 00-004-0806, W<sub>2</sub>C: 00-035-0776, WC: 00-025-1047)<sup>49-51</sup>**

### 3.3 Carbon monoxide chemisorption

CO chemisorption experiments were performed to obtain the CO uptake of the 4 different catalyst materials. These experiments were performed on a fresh catalyst directly after synthesis once the reactor was cooled down to 30 or 40 °C. A six port GC valve was attached just before the reactor upstream with one of the valve configurations connected to a line flowing a CO and argon mixture. The sample loop configuration of the 6 port valve is described in Figure 42 in Appendix I. The CO-Ar mixture was injected on the fresh catalyst surface. Several pulses were injected until the pulse area became constant which is where the surface got saturated, and no more CO could chemisorb on the carbide surface. The carbide was then subjected to a temperature-programmed

desorption from 40 °C to 250 °C and held for 20 min before the catalyst was again allowed to cool down. A desorption peak indicates the removal of the adsorbed CO from the surface.

### 3.4 High pressure toluene hydrogenation

Commercial toluene (99.8%) obtained from Sigma Aldrich was used to conduct the hydrogenation catalytic tests. Liquid toluene was flowed to the reactor using a Legato 011 SS continuous injection syringe pump with a maximum volume of 2 ml. Toluene flowrate for the reaction is maintained at 0.15 ml/hr. Ultra-high purity grade hydrogen (HY UHP 300) high pressure steel cylinder was obtained from Airgas.

The reactor was pressurized to 20 bar for the catalytic test reaction, and a back pressure regulator was used to pressurize the system to 20 bar. A Swagelok pressure gauge was attached to the reactor assembly to monitor and control the required pressure to the system. The H<sub>2</sub> flow was maintained at 75 ml/min (Bronkhorst STP). The temperature of reactor was ramped up to 160 °C and the toluene feed was introduced at this temperature to avoid any toluene feed condensation in the reactor and to ensure complete vaporization of the liquid. A GC injection was made at this temperature to ensure the detection of toluene and no other product peak formation at this temperature since product formation was found to occur at 200 °C. Once the toluene was detected in the mass spectrometer, the temperature was ramped up to 250 °C which was the desired reaction temperature.

The reaction products were monitored and analyzed using mass spectrometry and gas chromatography. A Varian CP3800 gas chromatograph was used for identification and quantification of the reaction products observed during the catalytic hydrogenation reaction. The gas chromatograph is equipped primarily with two detectors, namely flame ionization detector

(FID) and thermal conductivity detector (TCD). The compounds were separated over a PoraPLOT column. The GC-FID peak retention times provided information about the compound whereas the GC-FID areas of the products and toluene give a quantitative relationship based on conversion of toluene and the product yield and selectivity. Calibration experiments (Appendix I) were performed to obtain the response factors, relative response factors and retention times of the products that we expected to observe during our reaction. The sole product that is expected in toluene hydrogenation is methylcyclohexane whereas at higher temperatures ( $>300$  °C), methylcyclohexane ring cracking reaction and hydrogenolysis are observed to form methane as byproduct as evidenced by mass spectrometry profiles although we did not investigate this extensively at higher temperatures.

## CHAPTER 4

### RESULTS AND DISCUSSION

#### 4.1: Isothermal synthesis of tungsten carbide

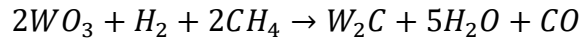
The synthesis of tungsten carbide is investigated in this work using an isothermal synthesis pathway. The volatile reduction products of tungsten trioxide precursor which are H<sub>2</sub>O and CO are monitored using mass spectrometry. These amounts of H<sub>2</sub>O and CO formed are then used to determine and describe the stoichiometry of the synthesis process. The tungsten carbide synthesis pathway in this work is explored with a parameter set composed of 4 different operating conditions. The carburization mixture is a 1:4 CH<sub>4</sub>:H<sub>2</sub> flow with a total flow of 38 ml/min. The parameter set for the different syntheses is as mentioned in Table 1. The mass spectrometry profiles for each of the synthesis mentioned in Table 1 are described in Figures 9-12.

**Table 1: Operating parameters for isothermal syntheses of tungsten carbide**

	Precursor material	Temperature (°C)	Precursor mass (mg)	Weight tungsten in precursor (mg)
Synthesis 1	WO <sub>3</sub> /SiO <sub>2</sub>	700	50	24.7
Synthesis 2	WO <sub>3</sub> /SiO <sub>2</sub>	750	50	24.7
Synthesis 3	WO <sub>3</sub>	700	30.5	24.2
Synthesis 4	WO <sub>3</sub>	750	30	23.8

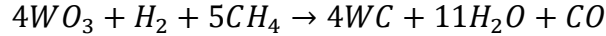
To describe the reduction carburization processes, we have formulated three possible stoichiometries based on the expected phases in the tungsten carbide system for the chemical reactions taking place through initial reduction of the precursor by hydrogen followed by methane.

a) Formation of  $W_2C$  from  $WO_3$ :



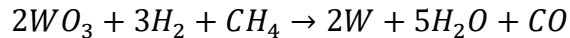
**Scheme 4: Stoichiometric reaction for formation of  $W_2C$  using  $WO_3$  precursor**

b) Formation of  $WC$  from  $WO_3$ :



**Scheme 5: Stoichiometric reaction for formation of  $WC$  using  $WO_3$  precursor**

c) Formation of metallic  $W$  from  $WO_3$ :



**Scheme 6: Stoichiometric reaction for formation of  $W$  using  $WO_3$  precursor**

The mass spectrometry profiles provide quantitative information on the gas phase vapor products evolved during the reduction-carburization process based on calibration data and some qualitative details highlighting the differences in the evolution profiles of the synthesis depending on the synthesis conditions employed. There is very little evidence as to how  $H_2$  consumption proceeds based on the profiles. Since  $H_2$  has a higher concentration in the carburization mixture, the consumption profile observed in the mass spectrometer showed only a small variation that was not easily quantifiable. Methane consumption can be visibly observed for all 4 synthesis conditions.

Synthesis 1:

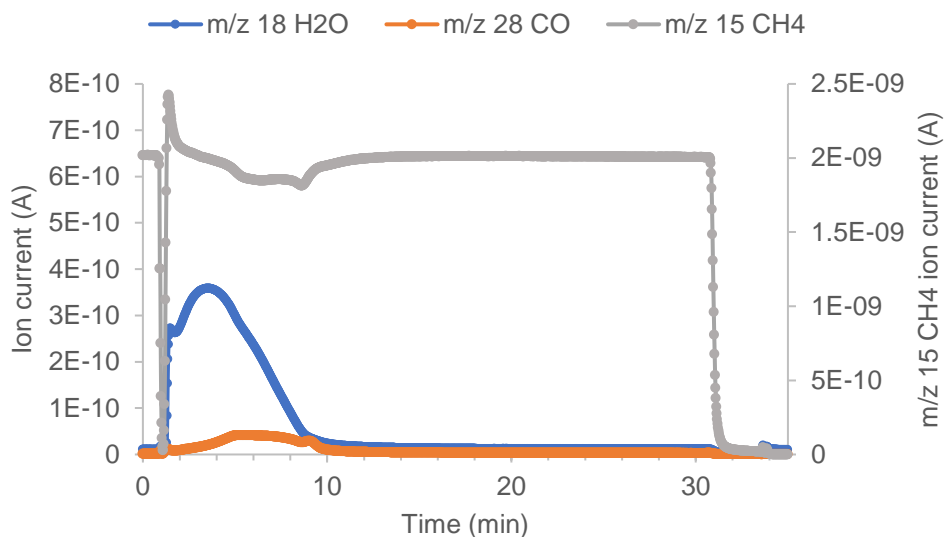


**Figure 9: Reduction signals at 700 °C isothermal period using a 50 mg WO<sub>3</sub>/SiO<sub>2</sub> precursor in a CH<sub>4</sub>/H<sub>2</sub> flow**

Synthesis 2:

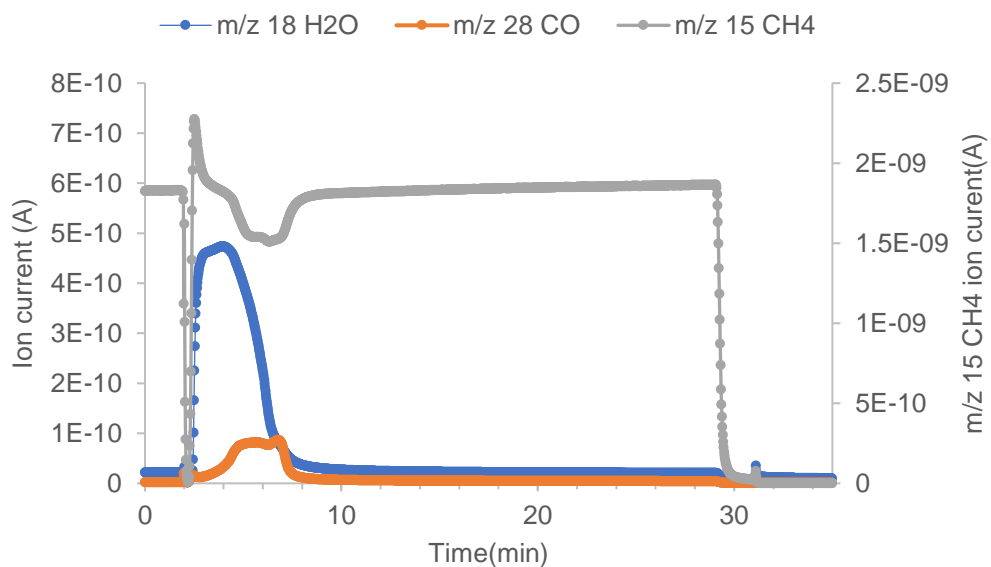


**Figure 10: Reduction signals at 750 °C isothermal period using a 50 mg WO<sub>3</sub>/SiO<sub>2</sub> precursor in a CH<sub>4</sub>/H<sub>2</sub> flow**

The high temperature synthesis profile indicates the reduction is faster as compared to the synthesis at 700 °C. At higher temperatures, the oxygen removal can be anticipated to proceed faster and that is further indicated by the H<sub>2</sub>O and CO profiles we observe at the syntheses at 750 °C using both silica-stabilized, and bulk precursor as observed in Figures 10, 12.

Synthesis 3:

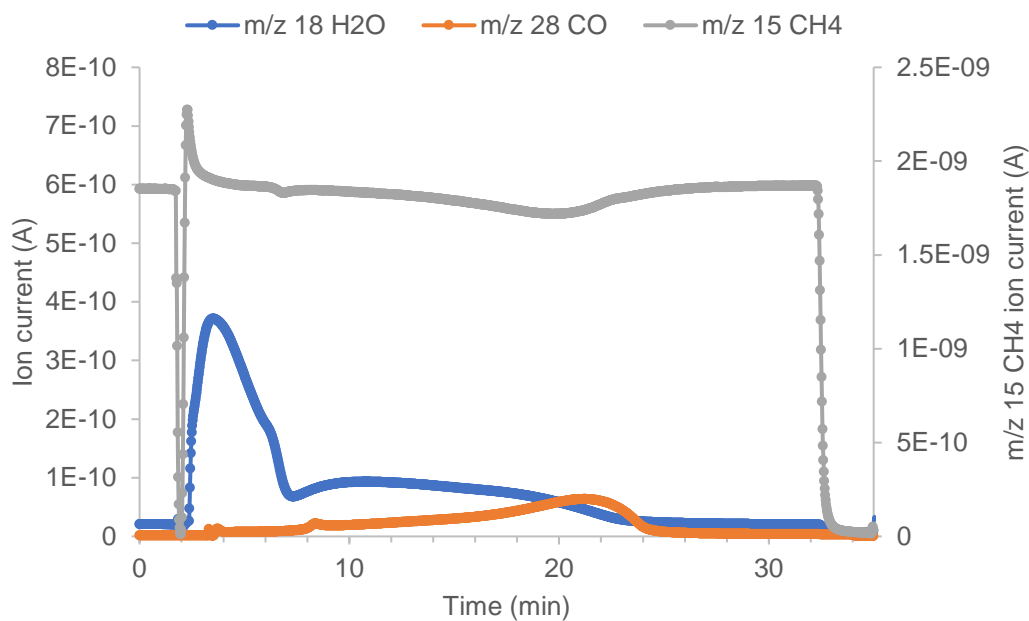


**Figure 11: Reduction signals at 700 °C isothermal period using a 30.5 mg bulk WO<sub>3</sub> precursor in a CH<sub>4</sub>/H<sub>2</sub> flow**

#### Synthesis 4:

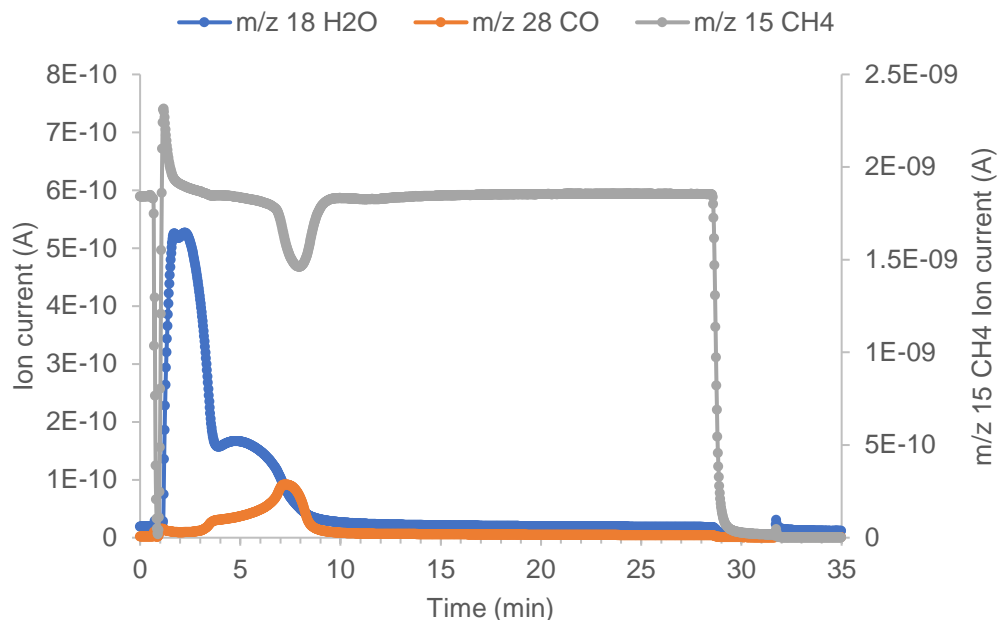


**Figure 12: Reduction carburization signals at 750 °C isothermal period using 30 mg bulk  $\text{WO}_3$  precursor in a  $\text{CH}_4/\text{H}_2$  flow**

The profiles of the reduction carburization process using a tungsten trioxide precursor show two different regions of activity in terms of  $\text{H}_2\text{O}$  and  $\text{CO}$  evolution profiles. These profiles hint towards the actual chemistry of the isothermal pathway that could be occurring during the reduction carburization process of the trioxide precursor. The peak profiles for methane coincide with the evolution of  $\text{CO}$  as observed in all the synthesis profiles.

Further, we evaluated the amounts of  $\text{H}_2\text{O}$  and  $\text{CO}$  formed during the syntheses using the calibration data described in Figures 38, 39 in Appendix I. Also, as can be observed in the mass spectrometry profiles, the reduction process is majorly dominated by the evolution of  $\text{H}_2\text{O}$  and only in the later stage of the synthesis does  $\text{CO}$  formation take place. The integrations of the synthesis signal peaks, and calculation of the amounts produced using the areas and calibration data made it possible to determine the amounts of  $\text{H}_2\text{O}$  and  $\text{CO}$  formed per mol  $\text{WO}_3$  precursor.

The amounts that are averaged for each type of synthesis over the number of syntheses are listed in Table 2.

**Table 2: Average amounts of H<sub>2</sub>O and CO produced per mmol WO<sub>3</sub> for the isothermal syntheses**

Precursor type	Synthesis temperature ( °C)	mmol H <sub>2</sub> O/mmol WO <sub>3</sub>	mmol CO/mmol WO <sub>3</sub>	mmol O /mmol WO <sub>3</sub>
WO <sub>3</sub> /SiO <sub>2</sub>	700	2.73	0.47	3.04
WO <sub>3</sub> /SiO <sub>2</sub>	750	2.55	0.60	3.01
WO <sub>3</sub>	700	2.48	0.72	3.03
WO <sub>3</sub>	750	2.69	0.51	3.07

Further the oxygen balance was calculated to evaluate the amount of oxygen that was taken up by H<sub>2</sub>O and CO in our syntheses in mmol O/mmol H<sub>2</sub>O or CO averaged over the number of syntheses for each of the 4 synthesis parameters. This oxygen balance is described in Figure 13.

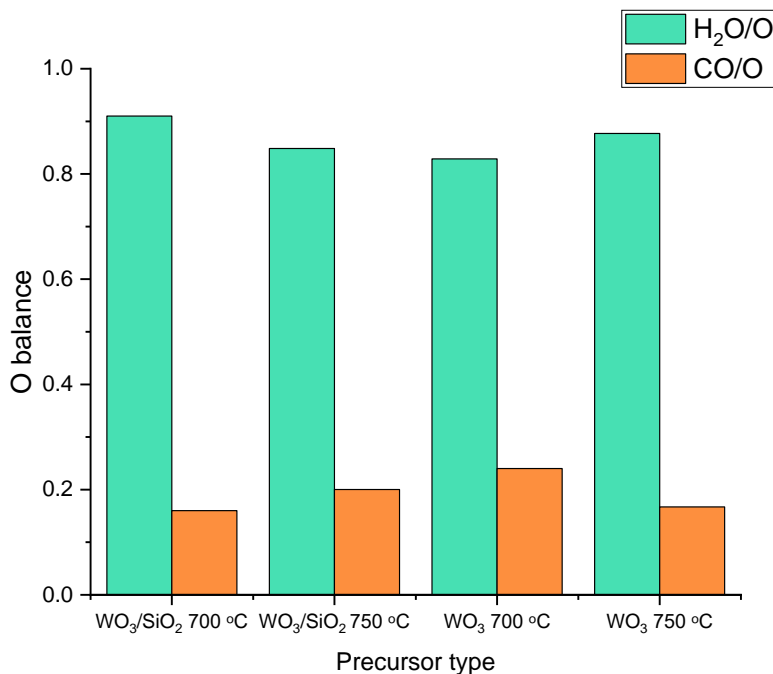


**Figure 13: Oxygen balance average for all 4 types of syntheses**

Although the balance does not equate 1, the evident trend is the fact that almost 80% of the oxygen in the starting precursor material goes to H<sub>2</sub>O, and the initial water formation is dominated by H<sub>2</sub> as no visible methane consumption was observed during the onset of the first water formation peak. That also suggests to the fact as observed by the MS profile that methane activation only takes place on a partially reduced oxide form of WO<sub>3</sub> (in essence WO<sub>3-x</sub>) since the onset of reduction is only activated by H<sub>2</sub>.

#### 4.2: X-ray characterization of the catalysts

Since, we established 4 different synthesis conditions resulting in 4 possible different types of structures, we evaluated these structures using X-ray diffraction to obtain information about the phase compositions of the catalysts. The X-ray diffraction results are matched with the reference peaks obtained from ICDD patterns and compiled in Figure 14.

As mentioned before, W<sub>2</sub>C exists in multiple phases, and the produced carbides indeed gave diffractograms that did not permit the distinction of β-W<sub>2</sub>C, α-W<sub>2</sub>C and ε-W<sub>2</sub>C. The powder pattern fitting software identified the most likely phases for the produced carbides, and for the scope of this work, we used the phases with space groups and lattice parameters mentioned in Table 3.

**Table 3: Phases and space groups used for XRD analysis<sup>37,52</sup>**

Phase	Space group	Lattice parameters a, Å	b, Å	c, Å
ε-W <sub>2</sub> C (No. 162)	$P\bar{3}1m$	5.19	5.19	4.74
α-WC (No. 187)	$P\bar{6}m2$	2.90	2.90	2.84
W (No. 229)	$Im\bar{3}m$	3.16	3.16	3.16

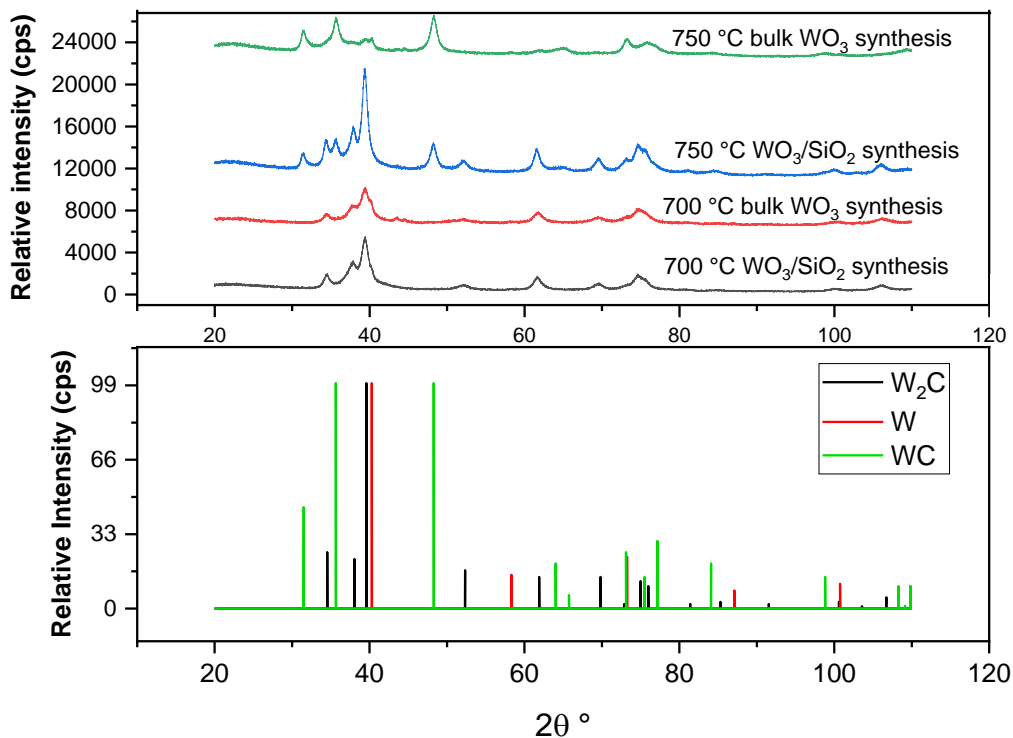


**Figure 14: Measured diffractograms for 4 syntheses with their stacked pattern references**

#### 4.2.1. Phase composition analysis of the catalysts

The diffractograms were further analyzed for their respective phase compositions using whole powder pattern fitting using Rigaku smartlab software. The selected range for the fitting was chosen from  $29^\circ$   $2\theta$  onwards to correct for any background inconsistency caused by silica/quartz wool pattern at  $25^\circ$   $2\theta$ . This characteristic silica appearance at the start of our diffractogram measurements is described in Figure 42 in Appendix I.

a) The powder pattern simulation of the diffractogram for a catalyst synthesized at a synthesis temperature of 700 °C using a  $\text{WO}_3/\text{SiO}_2$  precursor is described in Figure 15

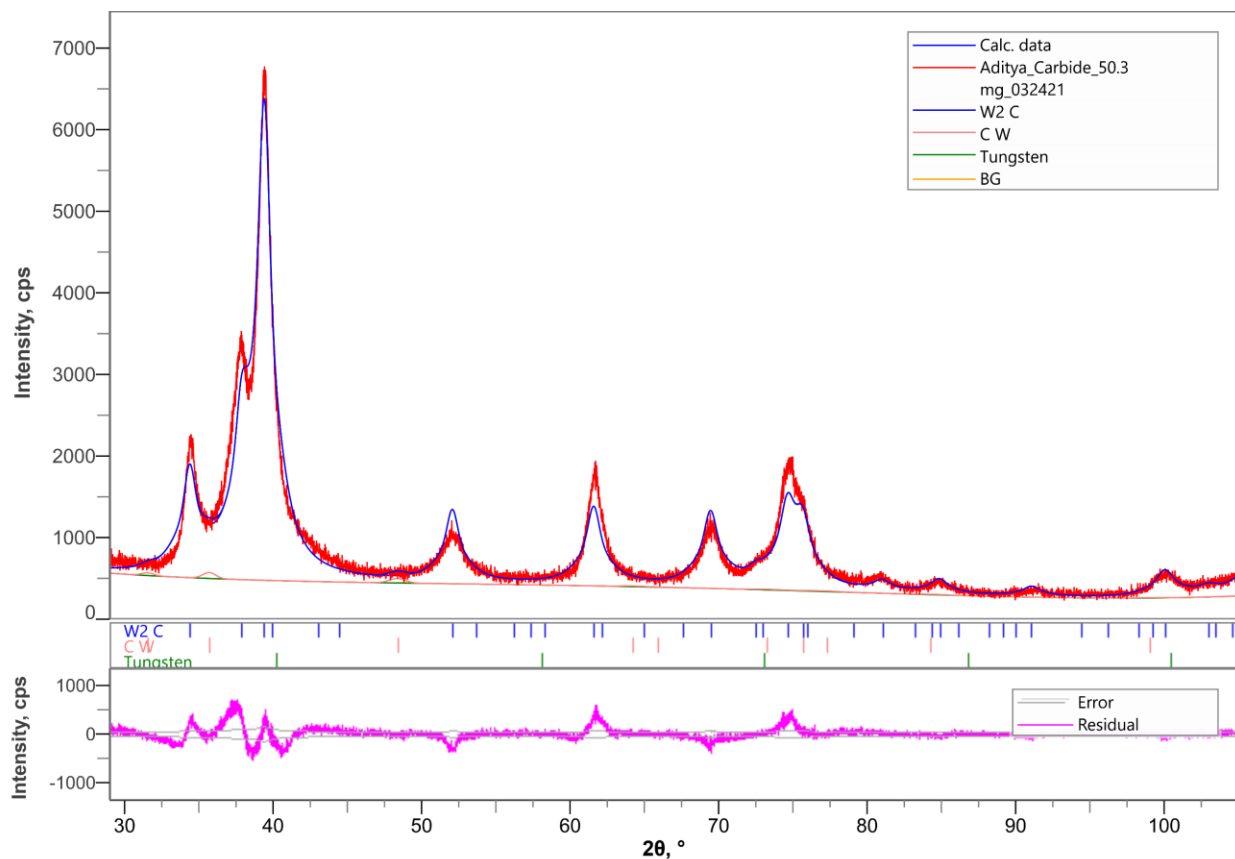


**Figure 15: XRD phase fitting of 700 °C synthesis using  $\text{WO}_3/\text{SiO}_2$  precursor**

The obtained fit for this sample using manual input parameters for lattice constants showed no metallic W contribution while little WC is detected at  $38^\circ 2\theta$  angle. The final phase composition achieved for this synthesis showed 98.8%  $\text{W}_2\text{C}$  and 1.2% WC. Thus, we ascertain that synthesis at 700 °C with the use of a silica-stabilized precursor results in a nearly phase pure  $\text{W}_2\text{C}$  catalyst.

b) Powder pattern simulation for a sample synthesized at 700 °C using a commercial WO<sub>3</sub> precursor is described in Figure 16

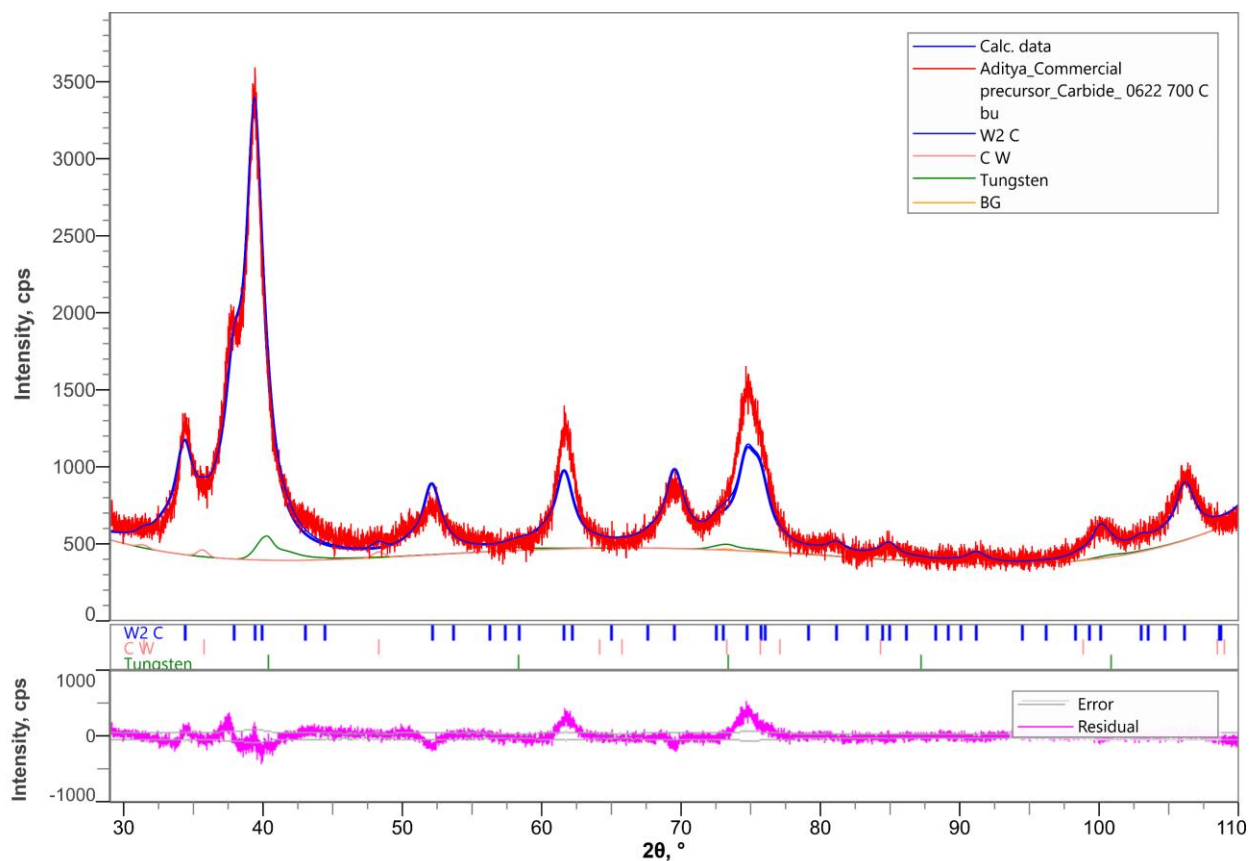


**Figure 16: XRD pattern fitting of a 700 °C synthesis using WO<sub>3</sub> bulk precursor**

The sample shows almost no WC contribution whereas little W is detected at 40° 2θ angle. The final phase composition achieved for this synthesis showed 95.9% W<sub>2</sub>C, 0.6% WC and 3.4% WC. Thus, even with a commercial precursor, we obtain a relatively W<sub>2</sub>C phase pure catalyst. Thus, the profound factor for the preference to a W<sub>2</sub>C phase is the synthesis temperature.

c) Powder pattern simulation for a catalyst synthesized at 750 °C using a  $\text{WO}_3/\text{SiO}_2$  precursor is described in Figure 17

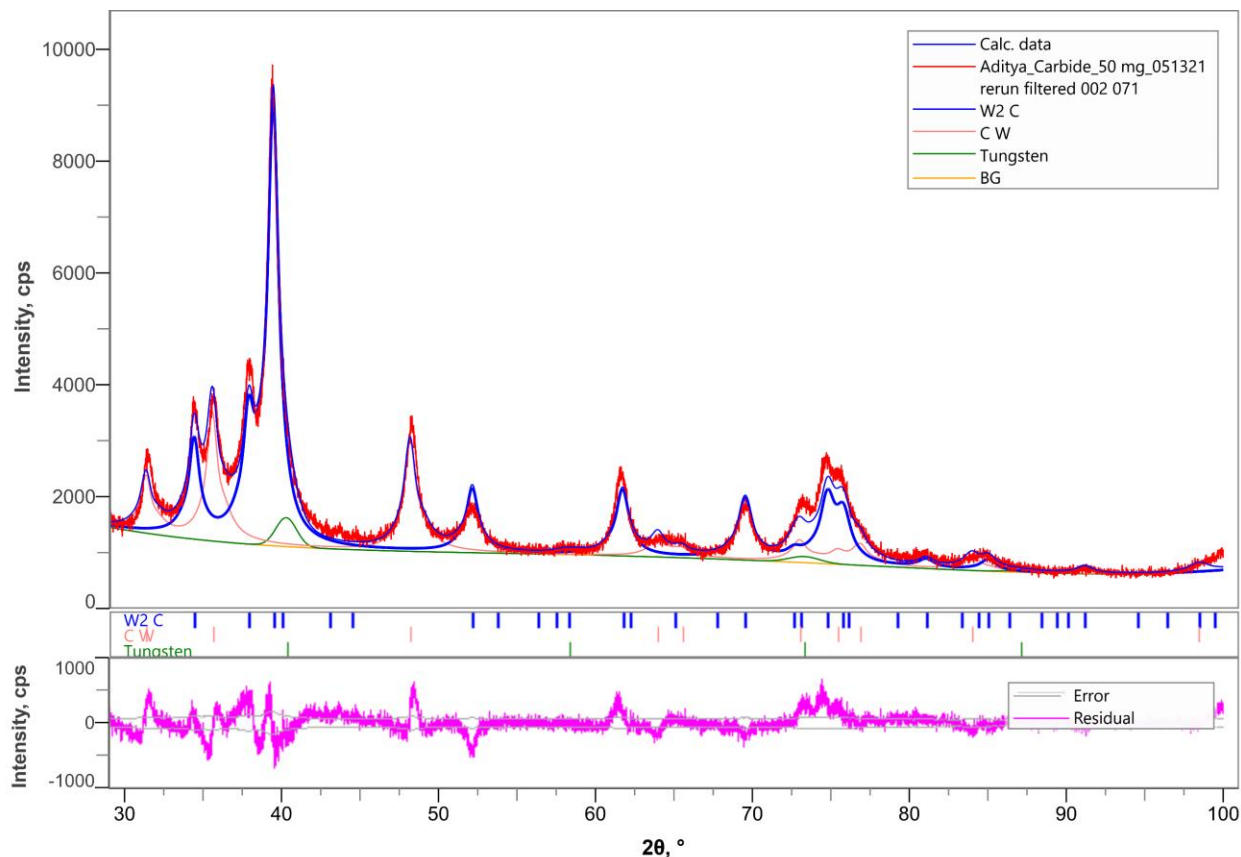


**Figure 17: XRD pattern fitting of a 750 °C synthesis using  $\text{WO}_3/\text{SiO}_2$  precursor**

The obtained fit for this sample using manual input parameters for lattice constants shows a phase composition comprising of a mixture of all three phases. The fit shows some residual which hints to some uncertainty in the convergence of the fit.

The final phase composition of the fit showed a contribution of 66.7%  $\text{W}_2\text{C}$ , 30.1% WC and 3.2% W metal. We observed that the increase in synthesis temperature tends to show increasing appearance of the monocarbide WC phase.

d) Powder pattern simulation for a catalyst synthesized at 750 °C using a commercial WO<sub>3</sub> precursor

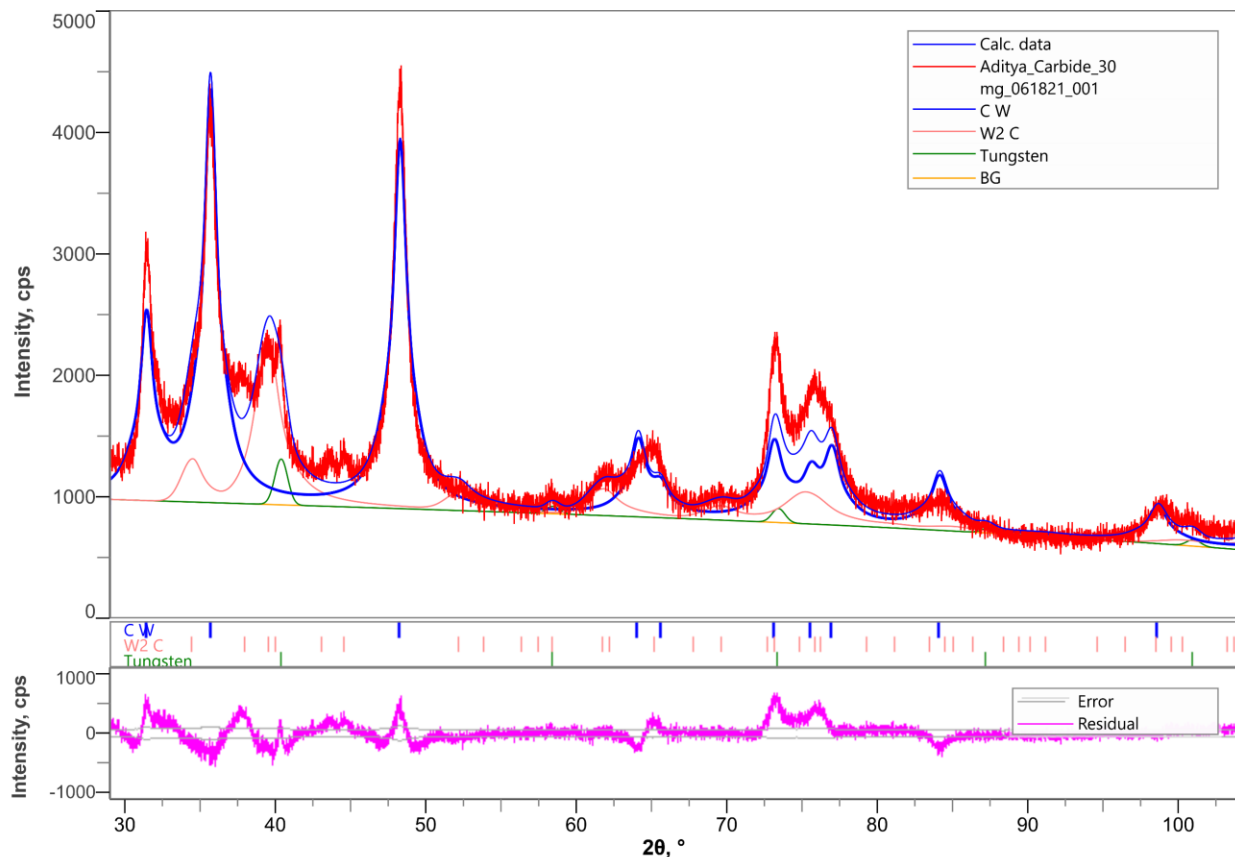


**Figure 18: XRD pattern fitting of a 750 °C synthesis using WO<sub>3</sub> precursor**

The obtained fit for this sample using manual input parameters for lattice constants also shows a phase composition comprising of a mixture of all three phase with a preference to WC. The fit shows a broad residual peak at  $2\theta$  range of 73-78° which adds some uncertainty to the convergence of the final fit. The final phase composition of the fit showed a contribution of 73.3% WC, 24.5% W<sub>2</sub>C and 2.2% W metal. Here, we observe that the increase in synthesis temperature and the absence of a silica-supported precursor tend to show majority appearance of the monocarbide WC phase with some W<sub>2</sub>C character.

#### 4.2.2 Crystallite size analysis:

The crystalline domain sizes of the particles of individual phases of WC and W<sub>2</sub>C were measured for some of the fitted patterns. Halder-Wagner (H-W) analysis was used to measure the crystallite sizes of the individual phases<sup>53</sup>. The size description is mentioned in Table 4 .

**Table 4: Crystalline domain sizes of WC and W<sub>2</sub>C particles**

Synthesis type	W <sub>2</sub> C size, nm	WC size, nm
700 °C WO <sub>3</sub> /SiO <sub>2</sub>	5.6	7
750 °C WO <sub>3</sub>	5.3	7.8

Thus, from the size analysis we can confirm that the W<sub>2</sub>C crystals lie in the range of 5-6 nm whereas the WC crystals are larger and lie in the range of 7-8 nm. Since the W<sub>2</sub>C crystals are smaller, and smaller particles suggest to larger surface area and increased catalytic activity, we hypothesized that the W<sub>2</sub>C rich phases from our synthesized catalysts should ideally be more catalytically active than the WC rich phases.

#### 4.2.3. Scanning electron microscopy(SEM) imaging:

The morphological features of the different carbide structures were interpreted using scanning electron microscopy which described magnified images of the surface topology and the possible dispersion of the W metal on the surface of tungsten carbide.

a) The surface features using SEM images of one of the catalysts synthesized at 700 °C using a bulk WO<sub>3</sub> precursor are described in Figure 19.

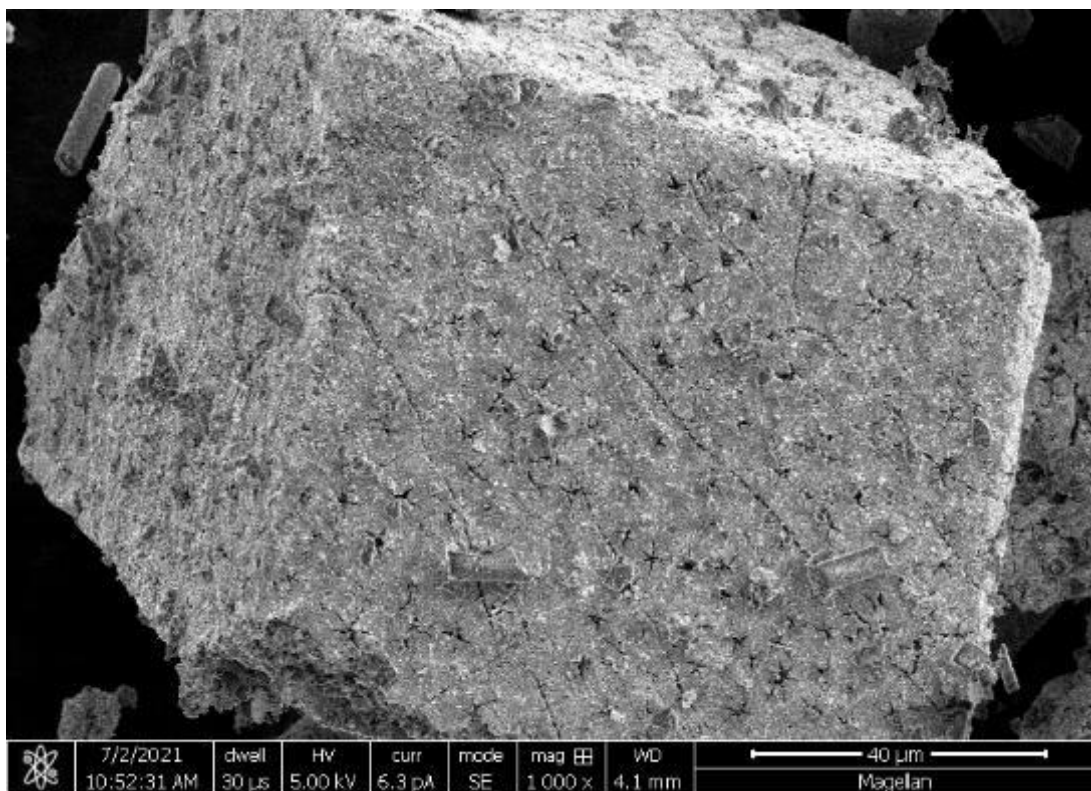


**Figure 19: Single crystal morphology of a tungsten carbide catalyst**

The image depicted the appearance of a particle in the tungsten carbide system. We see a particle with a cubic symmetry and sharp edges at the edge sites. Magnification into the surface helps understand features that are described in Figure 20.

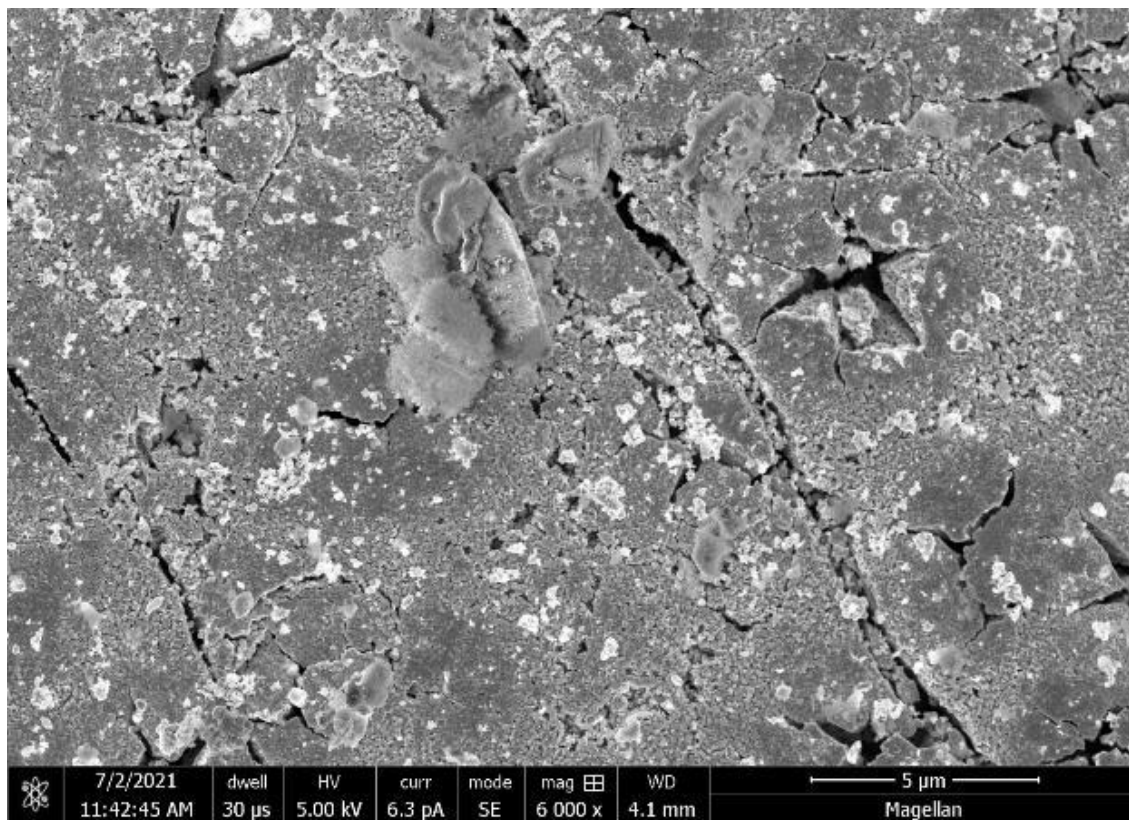


**Figure 20: Topological features of a tungsten carbide surface**

The surface features are prominently observed at higher magnifications on the surface of the catalyst. The bright particles on the surface could belong to either of the carbide phases or else the W metal since all three phases have metallic character. We can observe these particles with a metallic character dispersed over the surface whereas the rest of the surface could belong to the different carbide phases which can be indistinguishable but form the relatively darker area of the surface. The density of WC/W<sub>2</sub>C is twice that of the starting precursor WO<sub>3</sub>. Thus, the density increases as the carbide phases are being synthesized, and there is a considerable shrinkage in volume. This effect of volume shrinkage can be used to explain the formation of the tunnel like openings or crevices observed in Figure 20, which indicate the transformation of WO<sub>3</sub> to WC/W<sub>2</sub>C phases. Similar features of a carbide surface for a catalyst synthesized at 750 °C using bulk WO<sub>3</sub> are described in Figure 21.

b) SEM image of a tungsten carbide catalyst synthesized at 750 °C using bulk WO<sub>3</sub>

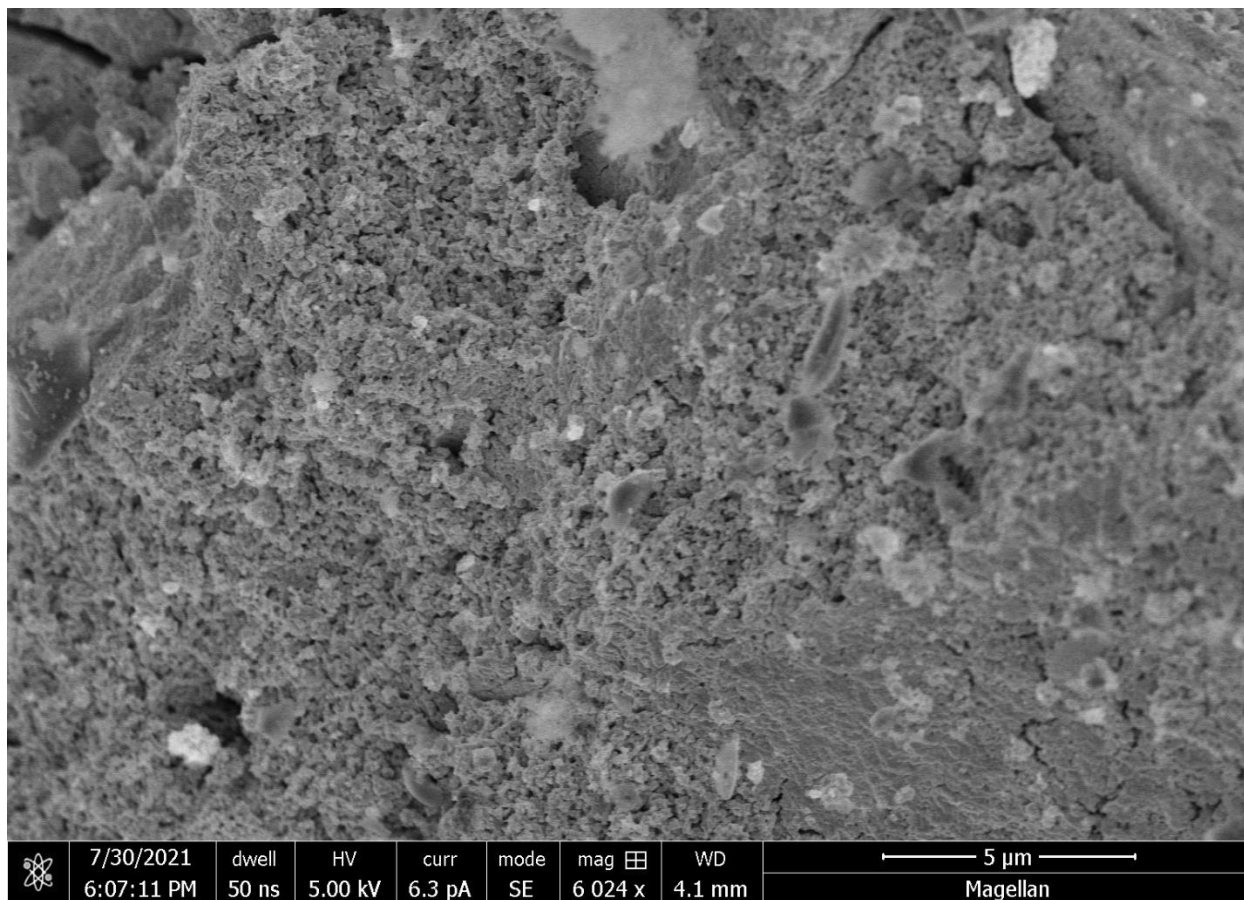


**Figure 21: SEM image of a tungsten carbide catalyst synthesized at 750 °C using bulk WO<sub>3</sub>**

This image showed a surface having relatively lesser metallic character in comparison to the previous image as observed by the distinct contrast between the brighter metallic particles dispersed over the surface.

### 4.3. Surface area determination using CO chemisorption analysis:

The use of silica precursor in the catalyst synthesis made use of N<sub>2</sub> physisorption surface area evaluation method inefficient as it also accounts for the silica area present in the precursor. As CO acts as a probe molecule that can selectively adsorb on the metallic carbide surface ignoring any silica surface, CO chemisorption analysis showed profound results of how the 4 different types of syntheses varied in their CO uptake areas.

The chemisorption was either performed at 30 or 40 °C, and a known concentration of CO:Ar gas mixture was pulsed several times on the catalyst surface until the surface was saturated, which can be confirmed by CO peaks of the same size. A TPD is then performed under inert flow of argon, and a desorption peak was observed depending on the total amount adsorbed during the pulses. A temperature timeline of the experiment is described in Figure 22. The pulse chemisorption is performed using mass spectroscopy and the mass/charge (m/z) ratio signal of 28 that belongs to CO is monitored during the pulses.

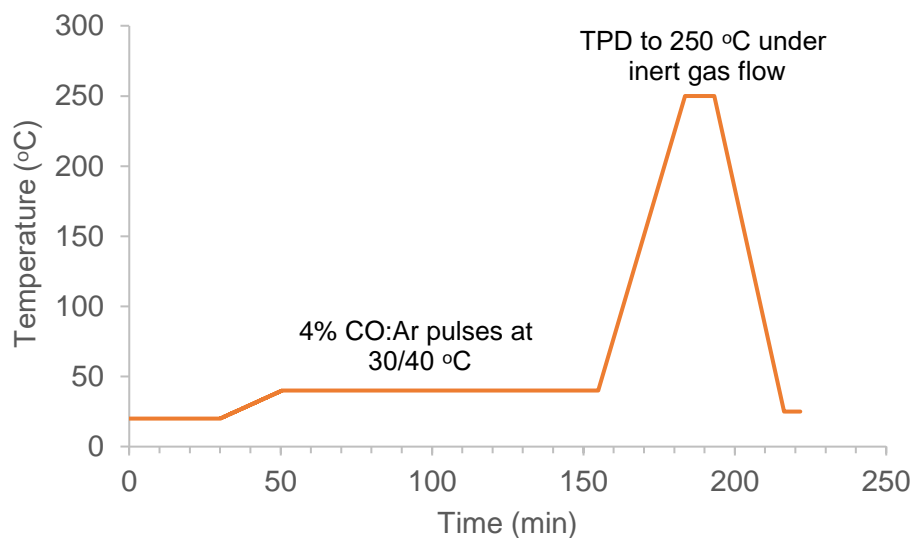


**Figure 22: Temperature timeline for a CO chemisorption experiment**

The nature of pulses for each of the 4 different syntheses and their cumulative CO adsorption plots are described in Figures 23-29.

a) CO chemisorption measurement for tungsten carbide catalyst synthesized at 700 °C using  $\text{WO}_3/\text{SiO}_2$  precursor:

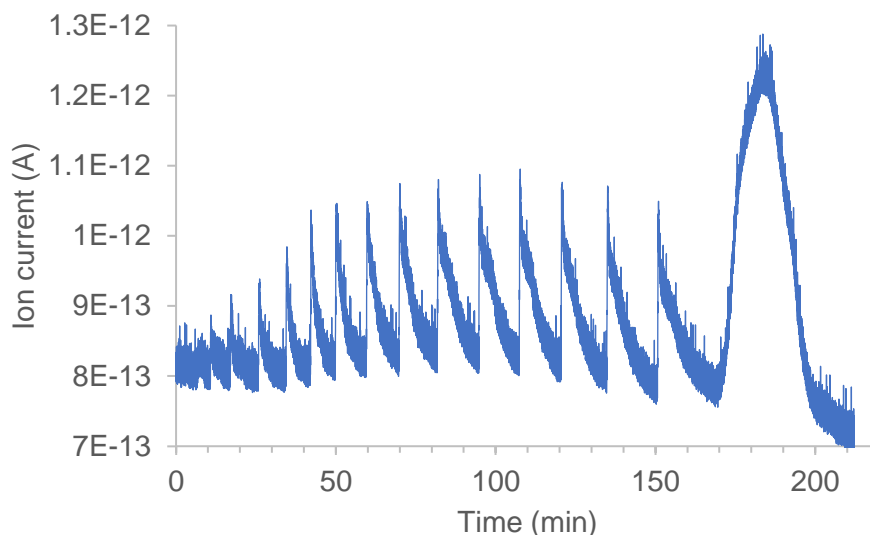


**Figure 23: CO chemisorption for a 700 °C  $\text{WO}_3/\text{SiO}_2$  precursor synthesis**

Broad peaks were observed for this sample with the first few pulses being almost completely adsorbed by the catalyst surface. The final few pulses are of the same size which denotes surface saturation. A TPD curve from 170-200 minutes period describes the desorbed amount of CO. The total CO uptake per mole W in the catalyst or the cumulative CO adsorbed (mol CO/mol W) over the number of pulses based on the peak areas and CO exposed to the surface as a function of the number of pulses is described in Figure 24. A sample calculation of the CO uptake measurement is described in Table 5 in Appendix I.

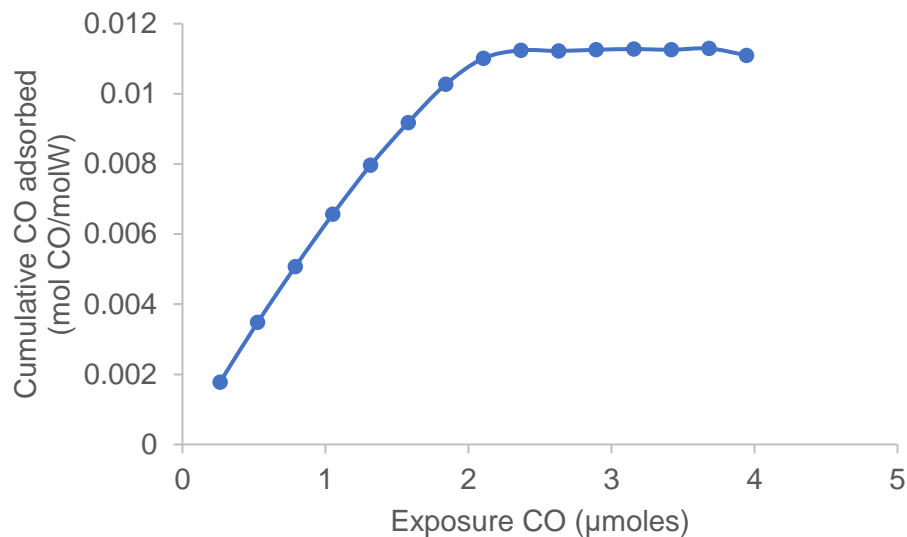


**Figure 24: Cumulative CO adsorption curve for a catalyst synthesized at 700 °C using  $WO_3/SiO_2$  precursor**

The cumulative plot explicitly describes the total  $\mu$ moles CO adsorbed by the catalyst during the pulses before being saturated. The sample resulted in a CO uptake of 0.011 mol CO/mol W, which was also the highest surface area amongst the 4 catalyst samples.

b) CO chemisorption measurement for tungsten carbide catalyst synthesized at 700 °C using bulk  $WO_3$  precursor:

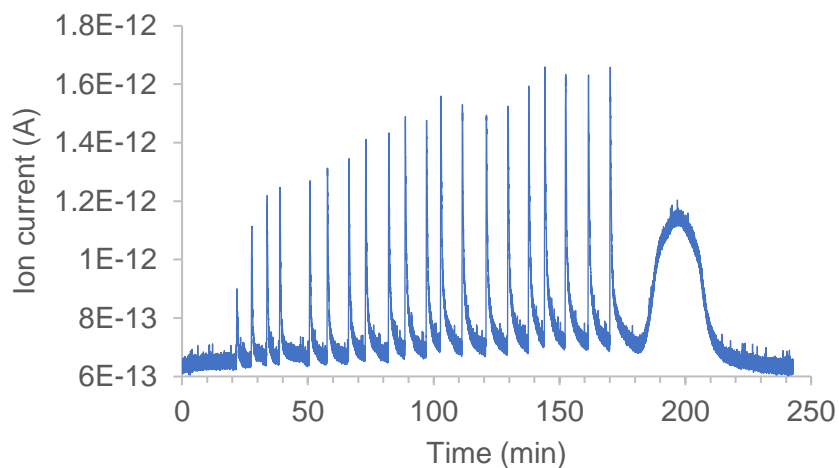


**Figure 25: CO chemisorption for a 700 °C bulk  $WO_3$  precursor synthesis**

This profile also shows how the first few pulses get adsorbed on the surface before eventually the peak size increases and becomes constant. The difference in this plot lies only in the nature of the peaks which are sharper and longer rather than wide and broad as for the high surface area catalyst.

A cumulative CO adsorption plot is further described in Figure 26 for this experiment.

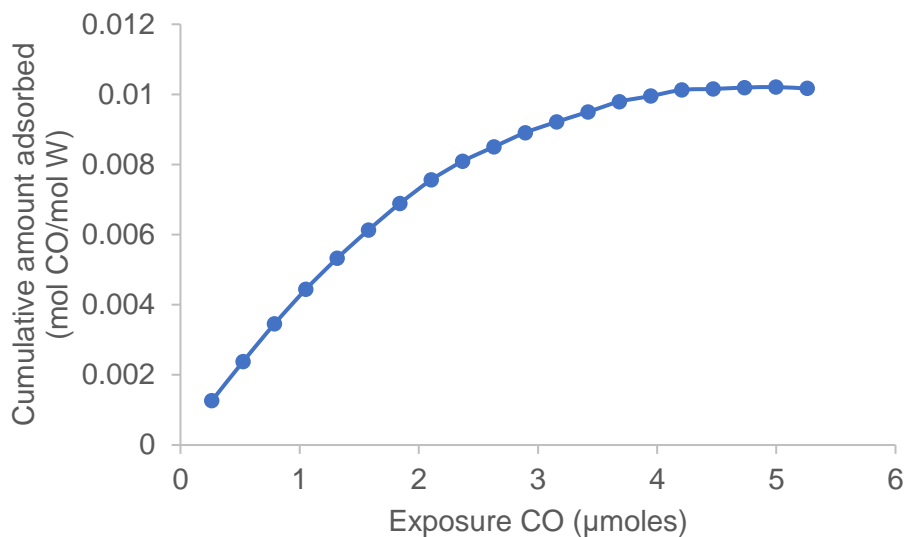


**Figure 26: Cumulative CO adsorption curve for a catalyst synthesized at 700 °C using a bulk  $\text{WO}_3$  precursor**

The sample resulted in an CO adsorption uptake of 0.00915 mol CO/mol W.

c) CO chemisorption measurement for tungsten carbide catalyst synthesized at 750 °C using  $\text{WO}_3/\text{SiO}_2$  precursor:

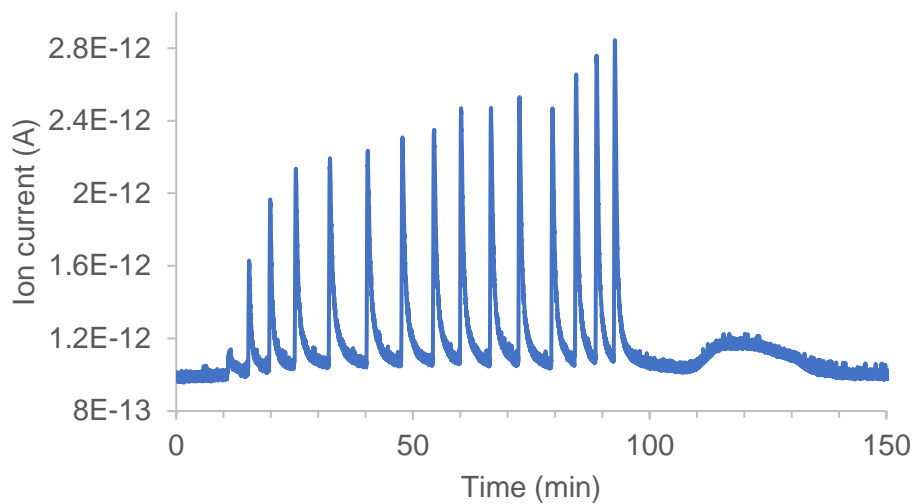


**Figure 27: CO chemisorption for a 750 °C  $\text{WO}_3/\text{SiO}_2$  precursor synthesis**

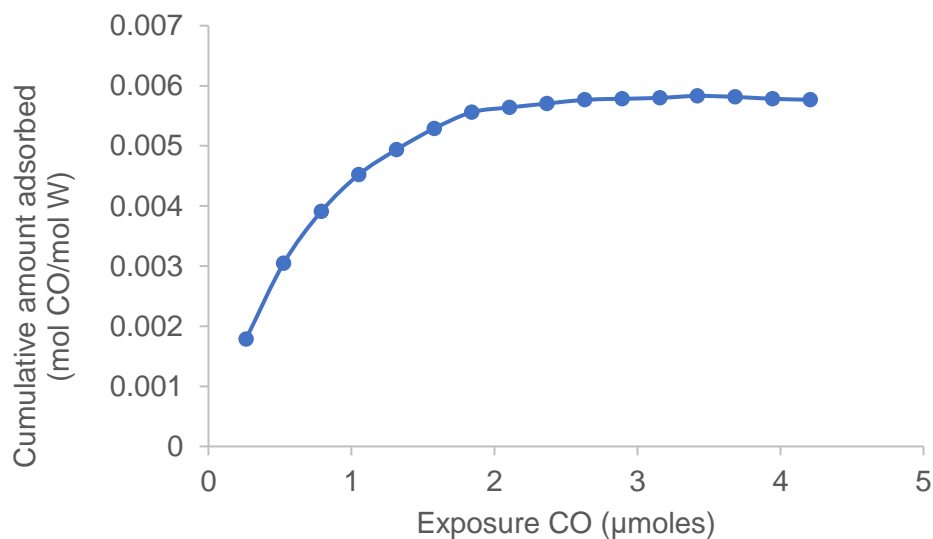


**Figure 28: Cumulative CO adsorption curve for a catalyst synthesized at 750 °C using a  $\text{WO}_3/\text{SiO}_2$  precursor**

This sample resulted in a CO uptake of 0.0054 mol CO/mol W.

d) CO chemisorption for tungsten carbide catalyst synthesized at 750 °C using bulk WO<sub>3</sub> precursor:

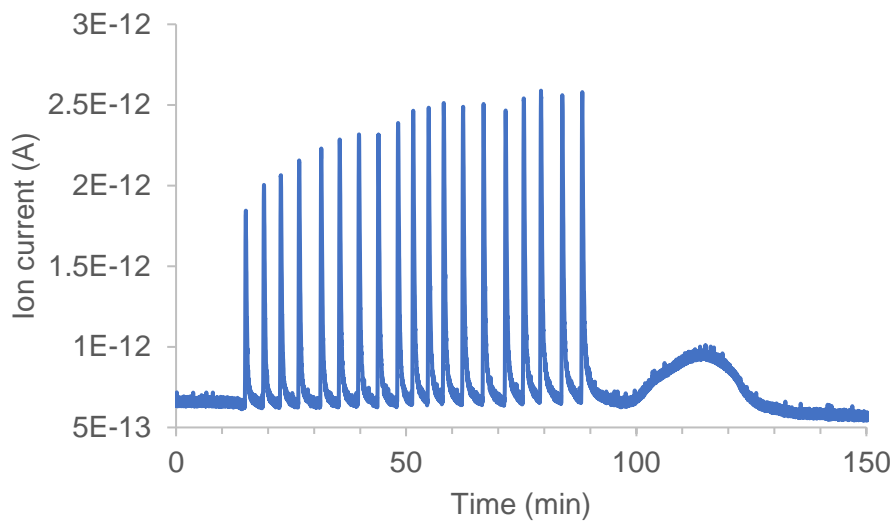


**Figure 29: CO chemisorption pulses for a sample synthesized at 750 °C bulk WO<sub>3</sub> precursor**

The profile explains how the first few pulses are short although not as small in comparison to the other 3 catalyst samples which further describes not much CO was adsorbed on this sample.

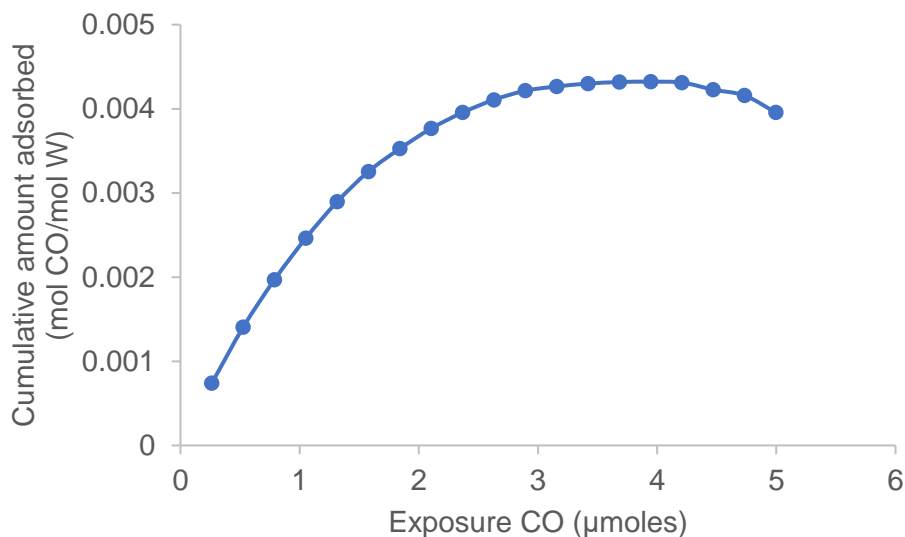


**Figure 30: Cumulative CO adsorption curve for a catalyst synthesized at 750 °C using a WO<sub>3</sub> precursor**

This sample resulted in a CO uptake of 0.0035 mol CO/mol W.

Thus, we formulated that the 4 different syntheses resulted in catalysts with varying surface areas as probed by CO chemisorption, and a combined cumulative plot for experiments done on each type of syntheses is presented in Figure 31.

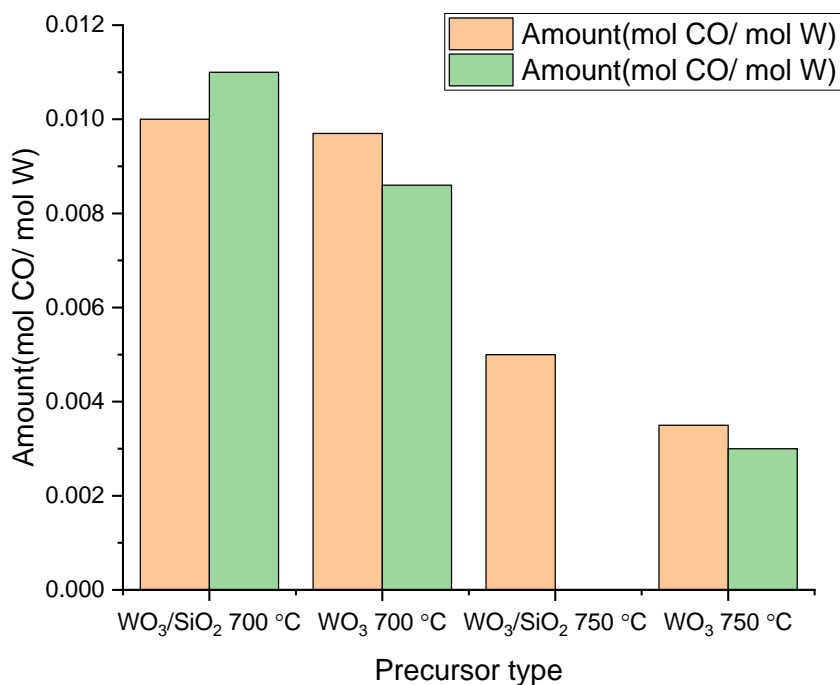


**Figure 31: CO adsorbed amounts for the 4 different catalyst syntheses conditions**

### 4.3. Toluene hydrogenation catalytic test reaction

The resulting catalysts based on the various synthesis conditions were evaluated for their toluene hydrogenation activities in the same packed bed steel tube reactor. The catalysis test was performed at a steady state temperature of 250 °C and a H<sub>2</sub>/ toluene ratio of 136 and a gauge pressure of 20 bar by adding H<sub>2</sub> to the toluene stream. The gauge pressure is set using a backpressure regulator.

The sole product was methylcyclohexane in all our catalytic tests, that is, the reaction was 100% selective to methylcyclohexane in the studied conditions for the catalysis. The rate of reaction was formulated as the rate of formation of methylcyclohexane per gram W per minute of reaction ( $\mu\text{mol.gW}^{-1}.\text{min}^{-1}$ ). Figure 32 describes the reaction rates obtained for all 4 of the synthesized catalyst materials normalized to the gram tungsten in the catalyst.

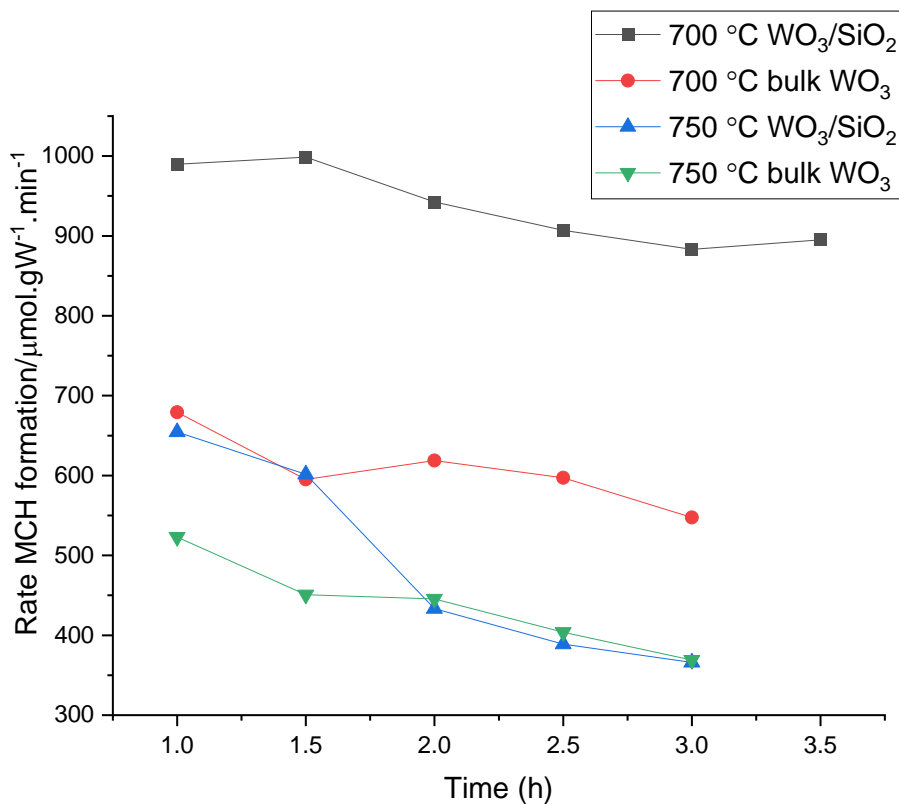


**Figure 32: Toluene hydrogenation activity of the 4 tungsten carbide catalysts**

In terms of the CO adsorption capacity of the catalysts, we evaluated a site time yield relationship based on the rate of reaction and the amount of  $\mu\text{mol}$  CO adsorbed for each catalyst.

This is further illustrated in Figure 33.

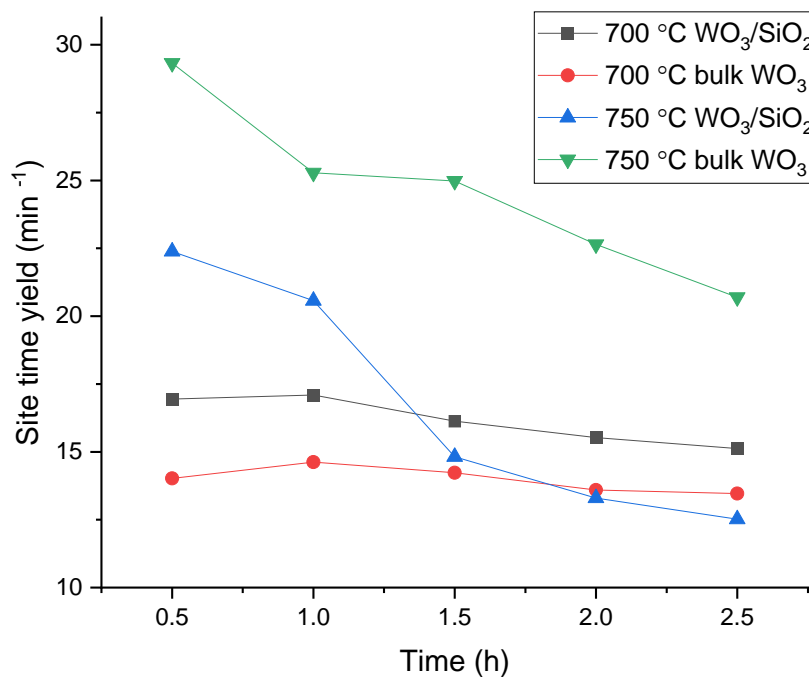


**Figure 33: Site time yield for the catalyst materials**

We also observed that a fresh catalyst and a catalyst for which CO chemisorption and TPD were performed differed in their activities, as shown in Figure 34.

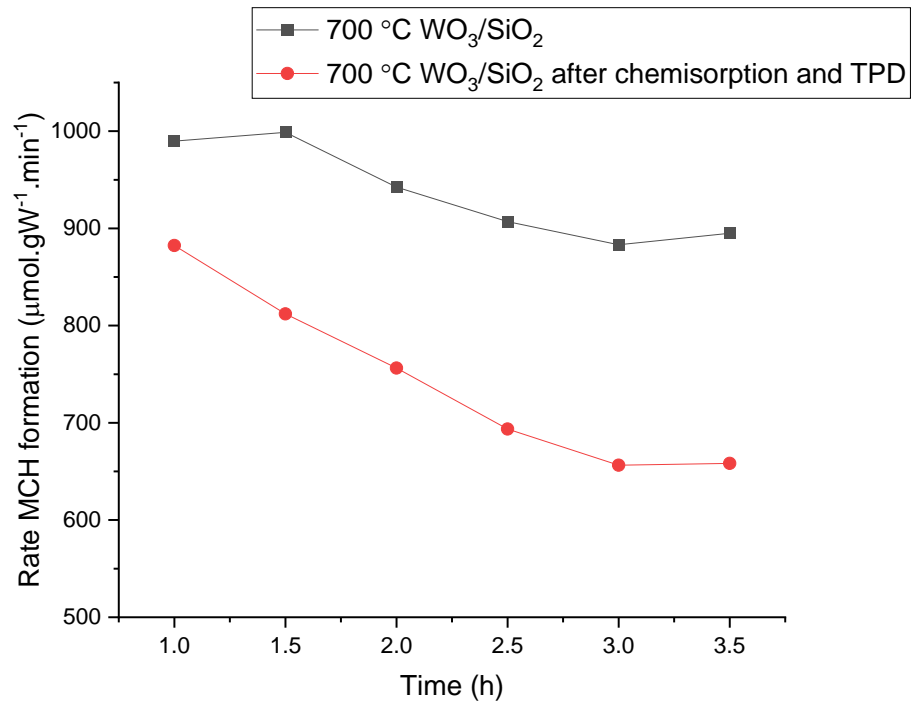


**Figure 34: Loss of activity of a fresh and chemisorption performed catalyst**

It could be hypothesized that the loss in activity stems from carbon removal from the surface during the temperature desorption as more amount of CO gets desorbed from the surface in contrast to what is adsorbed.

## CHAPTER 5

### SUMMARY AND CONCLUSION

Tungsten carbide as a material has been shown to behave similar to platinum for catalytic reactions. Although the usual high temperature synthesis makes the material ineffective for catalysis because of low surface areas. Also, since the tungsten carbide system is composed of two or more stoichiometries and phases that can be formed during the synthesis in a carburization atmosphere, it is essential to understand how to control specific phase compositions and still obtain high surface area materials. In this work, this characteristic feature of metal carbides has been studied for the tungsten carbide system in which we have successfully synthesized 4 different tungsten carbide phase compositions using synthesis temperatures and presence or absence of silica as process variables. The syntheses provide further understanding of the possible reaction stoichiometries of the reduction-carburization process in terms of  $H_2O$  and  $CO$  formation from the initial precursor. Further characterization of these 4 different syntheses proved how the catalysts differed in their phase mixtures, and this is summarized in Figure 35 that shows the phase compositions of each of the 4 catalyst materials.

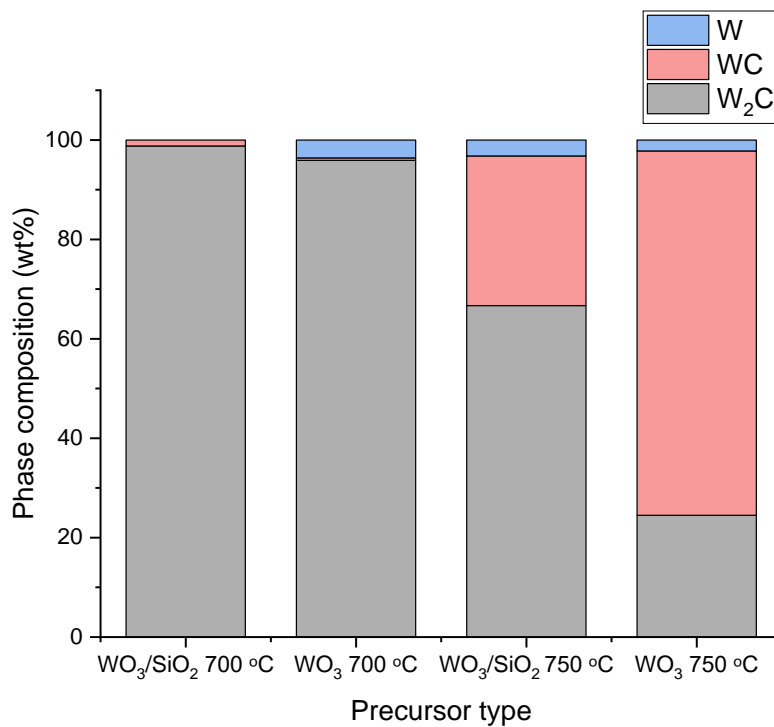


**Figure 35: Phase composition summary based on catalyst synthesis conditions**

Further, we observed the morphology of two of our catalyst samples using scanning electron microscopy and observed structural features that highlight some differences on a visual perspective, but there is not enough data to formulate any conclusions on the respective morphological differences of the two catalyst samples.

CO chemisorption analysis for surface areas of the 4 catalysts proved how the surface areas of the catalysts decreased as the synthesis temperatures were increased and the synthesis was conducted in the absence of the silica support for the precursor. The summarized plot showing the different CO uptake trends of the various WC/W<sub>2</sub>C catalysts is shown in Figure 36.

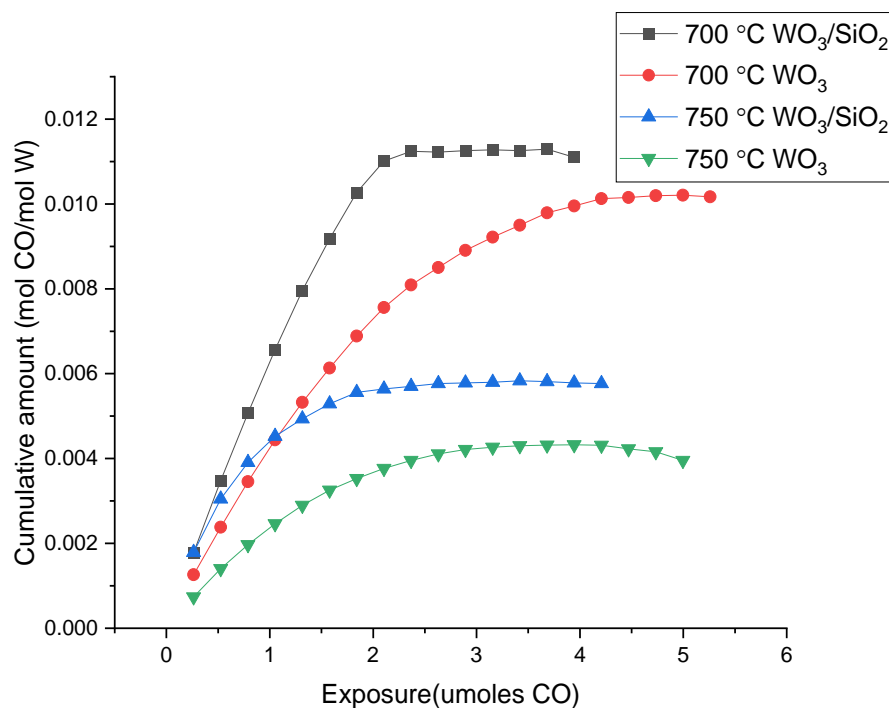


**Figure 36: CO adsorption capacity based on the catalyst synthesis conditions**

The W<sub>2</sub>C content was shown to influence the catalysts in terms of their surface areas. This is further summarized in Figure 37 which shows an increasing trend in terms of W<sub>2</sub>C weight % in the catalysts and their surface areas. Thus, we postulate that the W<sub>2</sub>C phase has higher catalytic activity per mass W although the intrinsic activity of the sites is not necessarily higher. The increase in activity with increasing W<sub>2</sub>C content is potentially a result of high carbidic surface area.

Catalytic tests proved that the catalysts with a W<sub>2</sub>C rich phase composition were more active for toluene hydrogenation and the activity dropped with the reduction in W<sub>2</sub>C content and the metallic surface area.

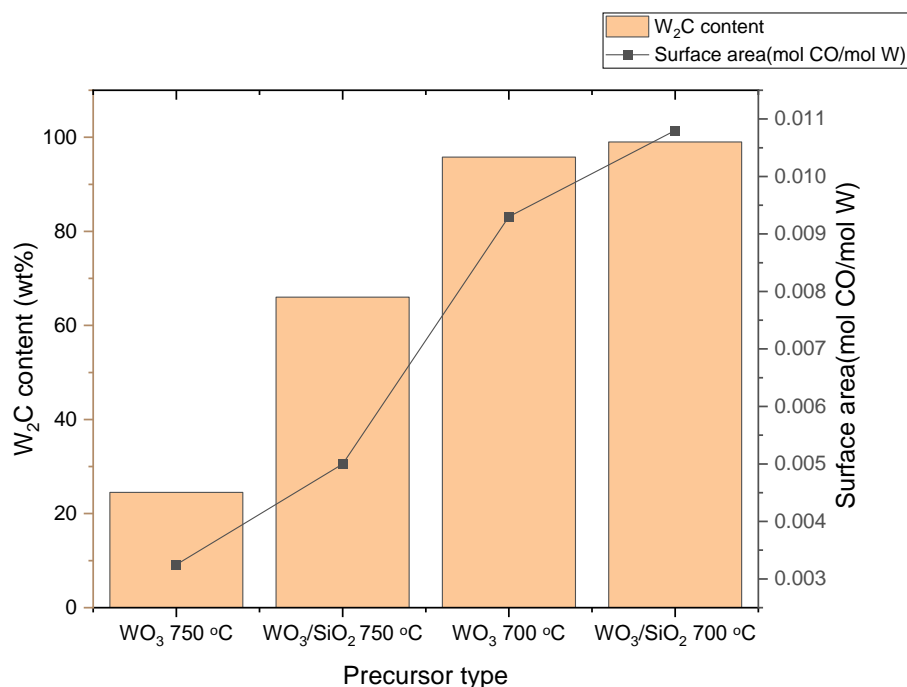


**Figure 37: Effect of increasing W<sub>2</sub>C content on surface area**

In conclusion, this work demonstrated the formation of 4 different phase compositions of tungsten carbide material based on the synthesis process parameters. The isothermal synthesis method was successful in stabilizing the W<sub>2</sub>C phase in the tungsten carbide structure for the synthesis done at 700 °C using a silica-stabilized precursor, and the obtained material showed high surface area and toluene hydrogenation activity.

Thus, we have shown in this work that an isothermal synthesis pathway is indeed beneficial for formation of high surface area tungsten carbide, and a correlation between the phase compositions of the synthesis, their surface areas and their catalytic activities was formulated.

## CHAPTER 6

### FUTURE WORK

The interesting chemistry of the isothermal reduction-carburization of tungsten trioxide to tungsten carbide needs some further exploration and refinement. The synthesis is influenced by the rates of  $H_2$  and  $CH_4$  consumption and with our synthesis protocol, we could not quantitatively determine these rates. This can be further investigated with betterment in the synthesis protocol and avoiding any signal overlaps. Optimization of the protocol will help collect concrete evidence for how different syntheses conditions will differ in the rates of  $H_2$  and  $CH_4$  consumption. Further understanding of the synthesis chemistry can be done using thermogravimetry analysis that will provide the rate of reduction of the precursor and interpretation of the phase transitions occurring during the reduction process based on weight loss of the initial precursor oxide.

A further optimization is required for the syntheses conditions to determine the parameters required to obtain a carbide catalyst which is WC phase pure since we could only synthesize a  $W_2C$  phase pure catalyst. The key to obtain such a material lies in avoiding excess carbon deposition on the surface while integrating more carbon into the bulk of the catalyst. The carburization gas mixture partial pressure and a higher  $CH_4$  concentration could possibly be the key for such a finding.

Some of the X-ray diffractograms show a good amount of residual in the final fits so a complete convergence of the fits is required to substantiate the final phase compositions and thus obtain the crystallite sizes of the individual phases.

The catalytic data shows significant scatter for the same type of catalysts for which the reasoning is unclear, and a certain number of measurements will be required to resolve this

uncertainty. Catalysis done under differential conditions will provide a better understanding of the reaction kinetics associated with toluene hydrogenation on tungsten carbide catalysts.

## Appendix I:

Calibration experiments for quantification of amounts (in moles) of H<sub>2</sub>O and CO produced during synthesis experiments.

### 1) H<sub>2</sub>O calibration (Figure 38):

The calibration for quantification of the reduction signal of H<sub>2</sub>O during synthesis was done based on injecting known amount of pulses by moles and integrating their peak areas as observed in the mass spectrometer. The plot shows a good correlation between the moles of pulses and the area distribution with a R<sup>2</sup> value of 0.998.

This analysis was then used to calculate the number of moles H<sub>2</sub>O produced for the 4 different syntheses that were performed.

These pulses were done in a gas flow of CH<sub>4</sub>:H<sub>2</sub> of 1:4, which was the same used during syntheses, and a temperature of 200 °C and atmospheric pressure.

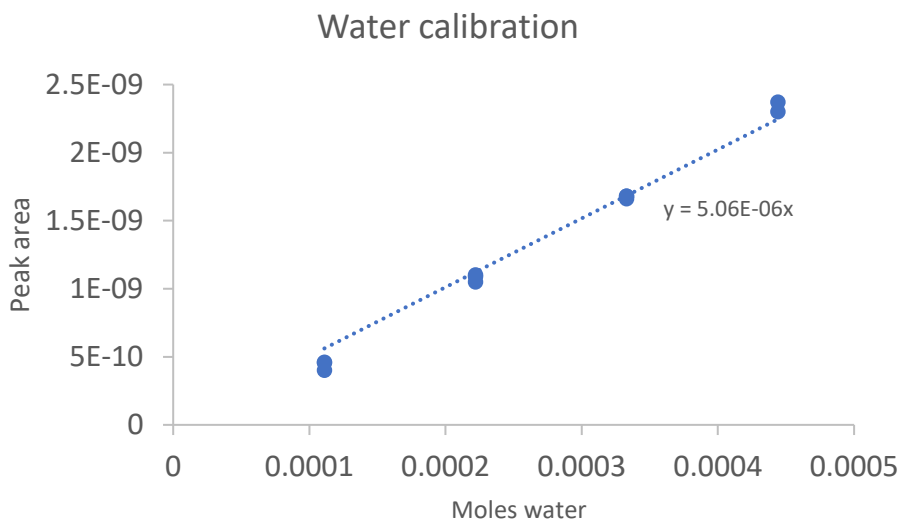


**Figure 38: Moles H<sub>2</sub>O injection pulses vs their respective peak areas of the ion current signals using mass spectrometry.**

2) CO calibration (Figure 39):

Similar to the calibration of H<sub>2</sub>O, similar pulses using a loop with known molar volume of CO mixed in an inert gas flow of Argon were performed and the resulting ion current signal peak areas were calculated. The plot below shows the calibration profile and a good correlation was obtained with an R<sup>2</sup> value of 0.9998.

This analysis was then used to calculate the amount of CO formed in moles, during the 4 different syntheses.

The pulses were performed in a series of 2, 3, 4 and 5% CO by concentration in a CO-Ar gas flow at a temperature of 40 °C and 1 atmospheric pressure.

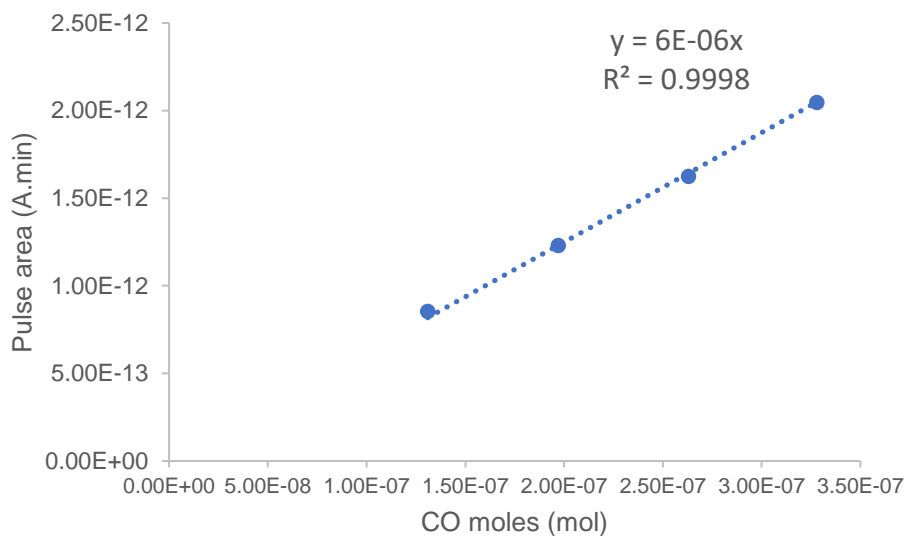


**Figure 39: Moles CO pulses vs their respective peak areas of the ion current signals using mass spectrometry.**

The CO calibration was further interpolated to a total flow of 38 ml/min used for the tungsten carbide synthesis. The interpolation resulted in a slope of 4.35E-06 which was further used to quantify the CO adsorbed amounts in the syntheses.

3) Uncertainties in quantitative interpretation of CH<sub>4</sub>, H<sub>2</sub> and CO<sub>2</sub> detection during synthesis:

The only quantifiable species during reduction of WO<sub>3</sub> precursor are H<sub>2</sub>O and CO. We observed negligible CO<sub>2</sub> formation during the syntheses which showed a signal intensity one order of magnitude lower than CO. The mass fragment of CO<sub>2</sub> is m/z 44 and is depicted by the light blue curve in Fig.40.

Similarly, the consumption of CH<sub>4</sub> and H<sub>2</sub> in this process could not be deduced because of the uncertain nature of the signal and difficulties in quantitative interpretation which was caused due to overlap with artifacts from valve switching. The initial changes in the trace could be a result of the gas streams switching from inert gas to carburizing gas mixture. The CH<sub>4</sub> mass fragment is m/z 15 indicated by the grey curve and H<sub>2</sub> mass fragment signal of m/z 3 is indicated by the yellow curve in Fig. 40.

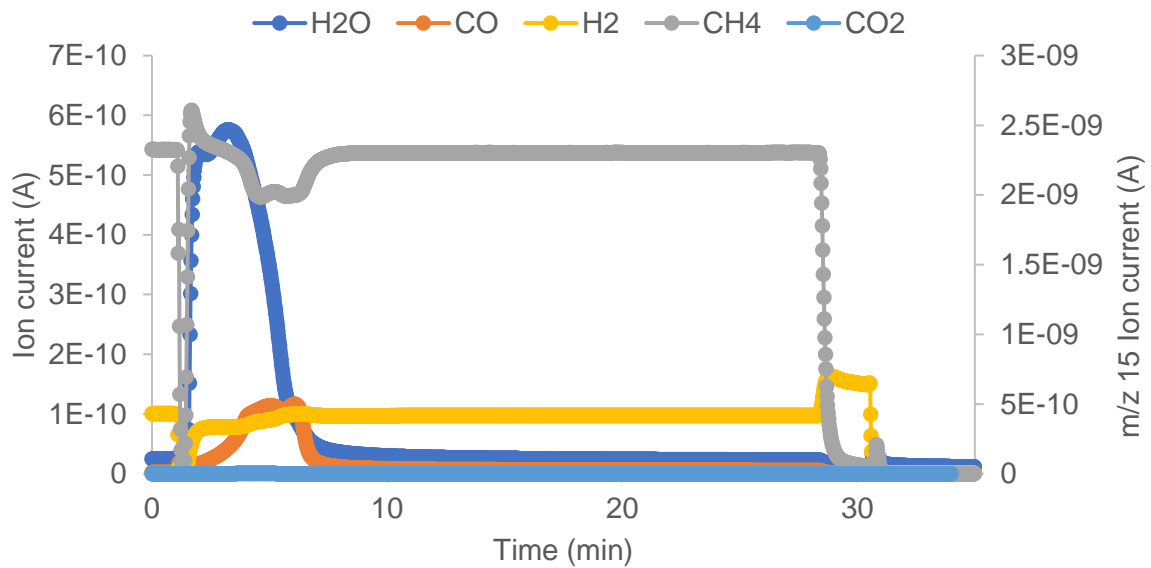


**Figure 40: Uncertain evidence for quantitative interpretation of CH<sub>4</sub>, H<sub>2</sub> consumption or CO<sub>2</sub> formation traces during synthesis period.**

- 4) Effect of condensation in the reactor stream on the formation of water signal in the MS  
 (Figure 41):

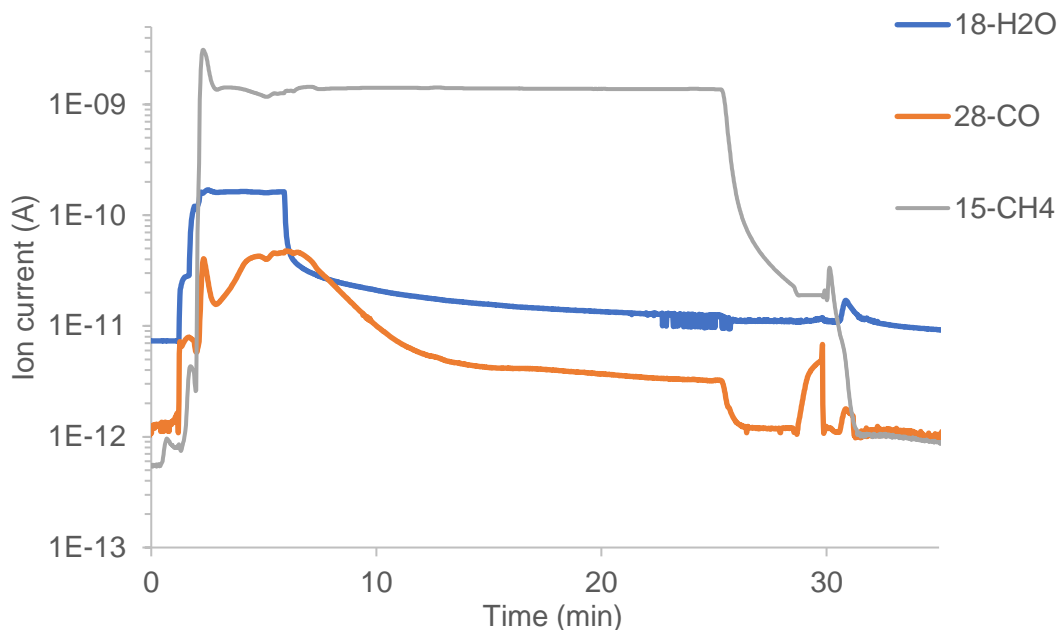


**Figure 41: Flat line nature of m/z 18 H<sub>2</sub>O signal during carbide synthesis**

- 5) 6 port valve description for CO chemisorption experiment (Figure 42):

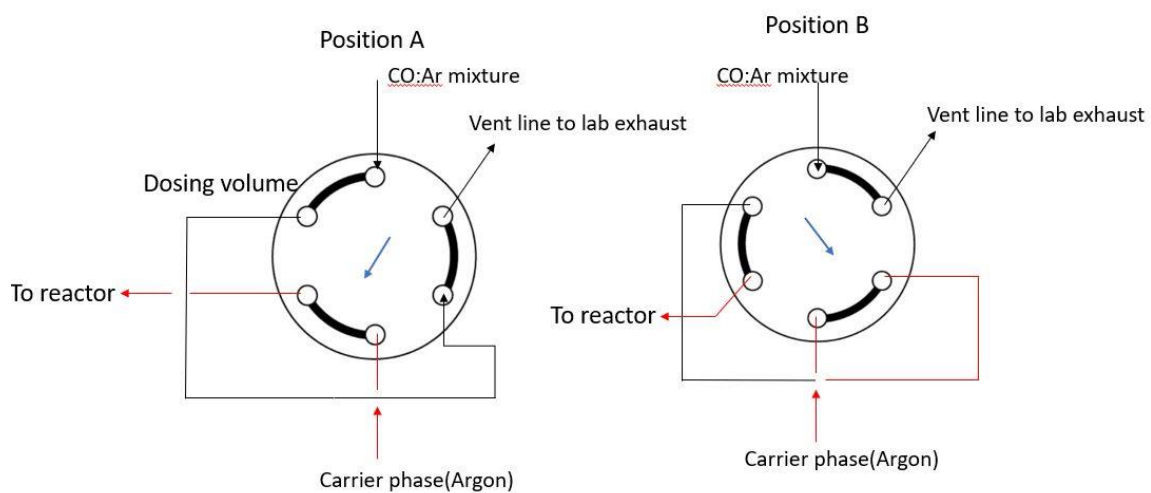


**Figure 42: 6 port GC valve configuration for CO chemisorption**

6) Silica background in the X-ray diffractograms (Figure 43):

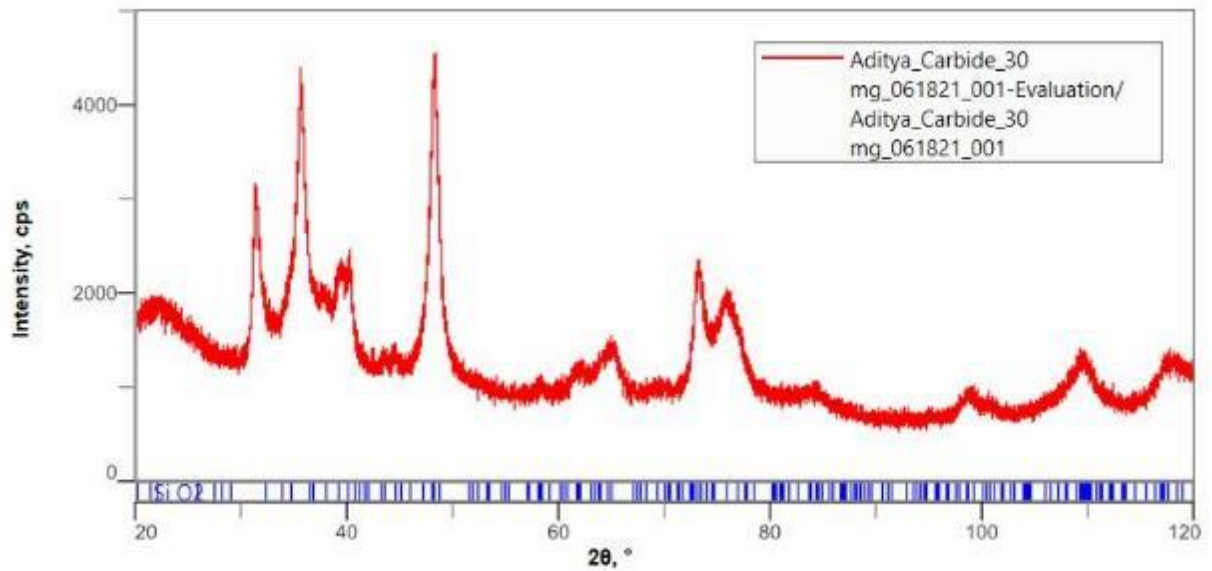


**Figure 43: Appearance of silica background at 20-25° 2θ**

As per the figure, we observed the silica peak at 20-25° 2θ. Since the tungsten carbide system has no reflections before 30° 2θ, the patterns were fit from 29° 2θ and onwards.

**Table 5: Sample CO chemisorption calculation template**

<b>A</b>	<b>B</b>	<b>C</b>	<b>D</b>	<b>E</b>	<b>F</b>	<b>G</b>	<b>H</b>
Pulse no	Peak area (A.min)	Adsorbed area	Cumulative area	Moles CO	Exposure( $\mu$ mol CO)	Cumulative CO (moles)	Cumulative amount (mol CO/mol W)
	Integrated area	Saturated area- B	$\sum_{i=1}^{16} (C)$	(100-(B/Sat.area) *pulse vol/100	A * Pulse vol *100	$\sum_{i=1}^{16} (G)$	G*10 <sup>6</sup> /1000 /mol catalyst
1	9.8E-14	1.12E-12	1.12E-12	2.42E-07	0.263	2.42E-07	0.001789
2	4.3E-13	7.9E-13	1.91E-12	1.7E-07	0.526	4.12E-07	0.003049
3	6.8E-13	5.4E-13	2.45E-12	1.16E-07	0.789	5.29E-07	0.00391
4	8.35E-13	3.85E-13	2.84E-12	8.3E-08	1.052	6.12E-07	0.004523
5	9.6E-13	2.6E-13	3.1E-12	5.6E-08	1.315	6.68E-07	0.004938
6	1E-12	2.2E-13	3.32E-12	4.74E-08	1.578	7.15E-07	0.005289
7	1.05E-12	1.7E-13	3.49E-12	3.66E-08	1.841	7.52E-07	0.00556
8	1.17E-12	5E-14	3.54E-12	1.08E-08	2.104	7.62E-07	0.00564
9	1.18E-12	4E-14	3.58E-12	8.62E-09	2.367	7.71E-07	0.005703
10	1.18E-12	4E-14	3.62E-12	8.62E-09	2.63	7.8E-07	0.005767
11	1.21E-12	1E-14	3.63E-12	2.16E-09	2.893	7.82E-07	0.005783
12	1.21E-12	1E-14	3.64E-12	2.16E-09	3.156	7.84E-07	0.005799
13	1.2E-12	2E-14	3.66E-12	4.31E-09	3.419	7.88E-07	0.005831
14	1.23E-12	-1E-14	3.65E-12	-2.2E-09	3.682	7.86E-07	0.005815
15	1.24E-12	-2E-14	3.63E-12	-4.3E-09	3.945	7.82E-07	0.005783
16	1.23E-12	-1E-14	3.62E-12	-2.2E-09	4.208	7.8E-07	0.005767

Volume of loop(pulse vol): 2.63E-07 mol

Saturated area(Sat.area): Average of the last 4 peaks. In this case :Avg(B13:B16) =1.225E-12

Total CO adsorbed: 7.8E-07 mol

Total CO desorbed: 8.2E-07 mol

## Appendix II:

### SAFETY CONSIDERATIONS

#### 5.1) Compressed gases:

The synthesis experiments involve flowing methane and hydrogen to the reactor at atmospheric pressure while the catalysis test involves running hydrogen at a pressure of 20 bar. The system is checked for leaks using a flammable gas leak detector always before running hydrogen in any of the experiments. The safety limits for the gases are mentioned in Table 6. The CO chemisorption experiment involves pulsing CO and argon gas in a controlled mixture or CO concentration and was performed according to the SOP guidelines as per the Jentoft lab and after personnel training on the equipment and handling.

**Table 6: Safety limits of gases used**<sup>54-56</sup>

Compressed gas	Exposure limit (ppm) (8 h)	Upper explosive limit (vol%)	Lower explosive limit (vol %)
H <sub>2</sub>	Unspecified	74	4
CH <sub>4</sub>	1000	16.4	4.4
CO	50	74	12.5

#### 5.2) Toluene material safety:

Explosive limits: 1.3(LEL)-7(UEL) vol%

The OSHA permissible exposure limit, ceiling and short-term exposure limit for toluene are 200 ppm (8 h period), 300 ppm and 500 ppm.<sup>57</sup>

### Handling:

Transfer of toluene into 20 ml vials is carried out in a fume hood with the proper PPE (safety glasses, gloves, and lab coats). The toluene vial is opened outside the fume hood for filling in the toluene injector syringe to fill around < 2 ml of toluene with proper PPE and the vial is then sealed and placed back in the storage cabinet.

## References:

- (1) Wijeyesekera, S. D.; Hoffmann, R. Transition-Metal Carbides. A Comparison of Bonding in Extended and Molecular Interstitials. *Organometallics* **1984**, 3(7), 949-961
- (2) Levy, R. B.; Boudart, M. Platinum-like Behavior of Tungsten Carbide in Surface Catalysis. *Science* **1973**, 181, 547-549. <https://doi.org/10.1126/science.181.4099.547>.
- (3) Pang, J.; Sun, J.; Zheng, M.; Li, H.; Wang, Y.; Zhang, T. Transition Metal Carbide Catalysts for Biomass Conversion: A Review. *Applied Catalysis B: Environmental*. **2019**, 254, 510-522. <https://doi.org/10.1016/j.apcatb.2019.05.034>.
- (4) Hou, R.; Chang, K.; Chen, J. G.; Wang, T. Replacing Precious Metals with Carbide Catalysts for Hydrogenation Reactions. *Topics in Catalysis* **2015**, 58, 240-246 <https://doi.org/10.1007/s11244-015-0365-1>.
- (5) Führer, M.; van Haasterecht, T.; Bitter, J. H. Molybdenum and Tungsten Carbides Can Shine Too. *Catalysis Science and Technology*. **2020**, 10, 6089-6097 <https://doi.org/10.1039/d0cy01420f>.
- (6) Li, Z.; Choi, J.-S.; Wang, H.; Lepore, A. W.; Connatser, R. M.; Lewis, S. A.; Meyer, H. M.; Santosa, D. M.; Zacher, A. H. Sulfur-Tolerant Molybdenum Carbide Catalysts Enabling Low-Temperature Stabilization of Fast Pyrolysis Bio-Oil. *Energy Fuels*. **2017**, 31, 9, 9585–9594. <https://doi.org/10.1021/acs.energyfuels.7b01707>.
- (7) Ma, J.; Zhu, S. G. Direct Solid-State Synthesis of Tungsten Carbide Nanoparticles from Mechanically Activated Tungsten Oxide and Graphite. *International Journal of Refractory Metals and Hard Materials* **2010**, 28 (5), 623–627. <https://doi.org/10.1016/J.IJRMHM.2010.06.004>.
- (8) Lausche, A. C.; Schaidle, J. A.; Schweitzer, N.; Thompson, L. T. Nanoscale Carbide and Nitride Catalysts. *Comprehensive Inorganic Chemistry II (Second Edition): From Elements to Applications* **2013**, 7, 371–404. <https://doi.org/10.1016/B978-0-08-097774-4.00730-0>.
- (9) Claridge, J. B.; York, A. P. E.; Brungs, A. J.; Green, M. L. H. Study of the Temperature-Programmed Reaction Synthesis of Early Transition Metal Carbide and Nitride Catalyst Materials from Oxide Precursors. *Chemistry of Materials* **2000**. 12(1), 132-142. <https://doi.org/10.1021/cm9911060>.
- (10) Leclercq, G.; Kamal, M.; Giraudon, J. M.; Devassine, P.; Feigenbaum, L.; Leclercq, L.; Frennet, A.; Bastin, J. M.; Löfberg, A.; Decker, S.; Dufour, M. Study of the Preparation of Bulk Powder Tungsten Carbides by Temperature Programmed Reaction with CH<sub>4</sub> + H<sub>2</sub> Mixtures. *Journal of Catalysis* **1996**. 158(1), 142-169 <https://doi.org/10.1006/jcat.1996.0015>.
- (11) Giraudon, J. M.; Devassine, P.; Lamonier, J. F.; Delannoy, L.; Leclercq, L.; Leclercq, G. Synthesis of Tungsten Carbides by Temperature-Programmed Reaction with CH<sub>4</sub>-H<sub>2</sub> Mixtures. Influence of the CH<sub>4</sub> and Hydrogen Content in the Carburizing Mixture. *Journal of Solid State Chemistry* **2000**. 154(2), 412-426 <https://doi.org/10.1006/jssc.2000.8859>.
- (12) Oyama, S. T. Preparation and Catalytic Properties of Transition Metal Carbides and Nitrides. *Catalysis Today* **1992**. 15(2), 179-200. [https://doi.org/10.1016/0920-5861\(92\)80175-M](https://doi.org/10.1016/0920-5861(92)80175-M).

- (13) Xiao, T.; Hanif, A.; York, A. P. E.; Sloan, J.; Green, M. L. H. Study on Preparation of High Surface Area Tungsten Carbides and Phase Transition during the Carburisation. *Physical Chemistry Chemical Physics* **2002**, *4*, 3522-3529. <https://doi.org/10.1039/b202518c>.
- (14) Mehdad, A.; Jentoft, R. E.; Jentoft, F. C. Passivation Agents and Conditions for Mo<sub>2</sub>C and W<sub>2</sub>C: Effect on Catalytic Activity for Toluene Hydrogenation. *Journal of Catalysis* **2017**, *347*, 89-101 <https://doi.org/10.1016/j.jcat.2017.01.002>.
- (15) Bretzler, P. Tungsten Carbide as Alternative for Precious Metal Based Hydrogenation- and Electrocatalysts, Dissertation, Technische Universität München, 2020.
- (16) Nasrallah M, D. Sintering Process and Catalysis. *International Journal of Nanomaterials, Nanotechnology and Nanomedicine* **2018**, *4*(1), 001–003. <https://doi.org/10.17352/2455-3492.000023>.
- (17) Chen, J. G. *Carbide and Nitride Overlayers on Early Transition Metal Surfaces: Preparation, Characterization, and Reactivities*; **1996**. *96*, *4*, 1477–1498. <https://doi.org/10.1021/cr950232u>
- (18) Mehdad, A.; Jentoft, R. E.; Jentoft, F. C. Single-Phase Mixed Molybdenum-Tungsten Carbides: Synthesis, Characterization and Catalytic Activity for Toluene Conversion. *Catalysis Today* **2019**, *323*, 112-122. <https://doi.org/10.1016/j.cattod.2018.06.037>.
- (19) Luković, J.; Babić, B.; Bučevac, D.; Prekajski, M.; Pantić, J.; Bašcarević, Z.; Matović, B. CERAMICS Synthesis and Characterization of Tungsten Carbide Fine Powders. *Ceramics International* **2015**, *41*, 1271–1277. <https://doi.org/10.1016/j.ceramint.2014.09.057>.
- (20) Wang, J.; Castonguay, M.; McBreen, P. H.; Ramanathan, S.; Oyama, S. T. Chemisorption of CO and NO on Molybdenum Carbide Foils. *The Chemistry of Transition Metal Carbides and Nitrides* **1996**, Chapter 23, 426–438. [https://doi.org/10.1007/978-94-009-1565-7\\_23](https://doi.org/10.1007/978-94-009-1565-7_23).
- (21) Choi, J. S.; Bugli, G.; Djéga-Mariadassou, G. Influence of the Degree of Carburization on the Density of Sites and Hydrogenating Activity of Molybdenum Carbides. *Journal of Catalysis* **2000**, *193* (2), 238–247. <https://doi.org/10.1006/JCAT.2000.2894>.
- (22) Boudart, M. Turnover Rates in Heterogeneous Catalysis. *Chemical Reviews* **1995**, *95* (3), 661-666. <https://doi.org/10.1021/cr00035a009>.
- (23) Castañ, P.; Arandes, J. M.; Pawelec, B.; Luis, J.; Fierro, G.; Gutiérrez, A.; Bilbao, J. Kinetic Model Discrimination for Toluene Hydrogenation over Noble-Metal-Supported Catalyst, *Ind. Eng. Chem. Res.* **2007**, *46*, *23*, 7417–7425. <https://doi.org/10.1021/ie070094m>.
- (24) Somorjai, G. A.; Carrazza, J. Structure Sensitivity of Catalytic Reactions; *Ind. Eng. Chem. Fundani*. **1986**, *25*, 63-69
- (25) Imada, T.; Iida, Y.; Ueda, Y.; Chiku, M.; Higuchi, E.; Inoue, H. Electrochemical Toluene Hydrogenation Using Binary Platinum-Based Alloy Nanoparticle-Loaded Carbon Catalysts. *Catalysts* **2021**, *11*(3), 318. <https://doi.org/10.3390/catal11030318>.
- (26) Salehzadeh, S.; Maleki, Farahnaz. The 4s and 3d Subshells: Which One Fills First in Progressing through the Periodic Table and Which One Fills First in Any Particular Atom? *Found Chem.* **2016**, *18*, 57–65. <https://doi.org/10.1007/s10698-016-9249-0>.
- (27) Bennett, L. H.; McAlister, A. J.; Watson, R. E. Interstitial Compounds. *Physics Today* **1977**, *30* (9), 34. <https://doi.org/10.1063/1.3037709>.

- (28) Zhong, Y.; Xia, X.; Shi, F.; Zhan, J.; Tu, J.; Fan, H. J. Transition Metal Carbides and Nitrides in Energy Storage and Conversion. *Adv. Sci.* **2016**, *3*, 1500286 <https://doi.org/10.1002/advs.201500286>.
- (29) Souza Macedo, L.; Teixeira Da Silva, V.; Bitter, J. H. Activated Carbon, Carbon Nanofibers and Carbon-Covered Alumina as Support for W2C in Stearic Acid Hydrodeoxygenation. *ChemEngineering*. **2019**, *3*(1), 24. <https://doi.org/10.3390/chemengineering3010024>.
- (30) Lee, W. S.; Wang, Z.; Wu, R. J.; Bhan, A. Selective Vapor-Phase Hydrodeoxygenation of Anisole to Benzene on Molybdenum Carbide Catalysts. *Journal of Catalysis* **2014**, *319*, 44–53. <https://doi.org/10.1016/J.JCAT.2014.07.025>.
- (31) Sullivan, M. M.; Chen, C.-J.; Bhan, A. Catalytic Deoxygenation on Transition Metal Carbide Catalysts. *Catalysis Science & Technology* **2016**, *6* (3), 602–616. <https://doi.org/10.1039/C5CY01665G>.
- (32) Medeiros, F. F. P.; de Oliveira, S. A.; de Souza, C. P.; da Silva, A. G. P.; Gomes, U. U.; de Souza, J. F. Synthesis of Tungsten Carbide through Gas–Solid Reaction at Low Temperatures. *Materials Science and Engineering: A* **2001**, *315* (1–2), 58–62. [https://doi.org/10.1016/S0921-5093\(01\)01214-X](https://doi.org/10.1016/S0921-5093(01)01214-X).
- (33) Decker, S.; Lofberg, A.; Bastin, J.-M.; Frennet, A. Study of the Preparation of Bulk Tungsten Carbide Catalysts with C<sub>2</sub>H<sub>6</sub>/H<sub>2</sub> and C<sub>2</sub>H<sub>4</sub>/H<sub>2</sub> Carburizing Mixtures. *Catalysis Letters* **1997**, *44*, 229–239 <https://doi.org/10.1023/A:1018985227289>
- (34) Suetin, D. v.; Shein, I. R.; Ivanovskii, A. L. Structural, Electronic Properties and Stability of Tungsten Mono- and Semi-Carbides: A First Principles Investigation. *Journal of Physics and Chemistry of Solids* **2009**, *70* (1), 64–71. <https://doi.org/10.1016/J.JPCS.2008.09.004>.
- (35) Kurlov, A. S.; Gusev, A. I. Tungsten Carbides and W-C Phase Diagram. *Inorganic Materials* **2006**. *42*, 121–127. <https://doi.org/10.1134/S0020168506020051>.
- (36) Kurlov, A. S.; Gusev, A. I. Phase Equilibria in the W–C System and Tungsten Carbides. *Russian Chemical Reviews* **2006**. *75* (7), 617 <https://doi.org/10.1070/rc2006v075n07abeh003606>.
- (37) Shrestha, A.; Gao, X.; Hicks, J. C.; Paolucci, C. Nanoparticle Size Effects on Phase Stability for Molybdenum and Tungsten Carbides. *Chemistry of Materials* **2021**, *33* (12), 4606–4620. <https://doi.org/10.1021/acs.chemmater.1c01120>.
- (38) Szymańska-Kolasa, A.; Lewandowski, M.; Sayag, C.; Brodzki, D.; Djéga-Mariadassou, G. Comparison between Tungsten Carbide and Molybdenum Carbide for the Hydrodenitrogenation of Carbazole. *Catalysis Today* **2007**, *119* (1–4), 35–38. <https://doi.org/10.1016/J.CATTOD.2006.08.039>.
- (39) Gong, Q.; Wang, Y.; Hu, Q.; Zhou, J.; Feng, R.; Duchesne, P. N.; Zhang, P.; Chen, F.; Han, N.; Li, Y.; Jin, C.; Li, Y.; Lee, S. T. Ultrasmall and Phase-Pure W<sub>2</sub>C Nanoparticles for Efficient Electrocatalytic and Photoelectrochemical Hydrogen Evolution. *Nature Communications* **2016**. *7*, 13216. <https://doi.org/10.1038/ncomms13216>.
- (40) Huang, J.; Hong, W.; Li, J.; Wang, B.; Liu, W. High-Performance Tungsten Carbide Electrocatalysts for the Hydrogen Evolution Reaction. *Sustainable Energy & Fuels* **2020**, *4* (3), 1078–1083. <https://doi.org/10.1039/C9SE00853E>.
- (41) Yang, X. G.; Wang, C. Y. Nanostructured Tungsten Carbide Catalysts for Polymer Electrolyte Fuel Cells. *Applied Physics Letters* **2005**, *86* (22), 224104 <https://doi.org/10.1063/1.1941473>.

- (42) Stoffels, M. A.; Klauck, F. J. R.; Hamadi, T.; Glorius, F.; Leker, J. Technology Trends of Catalysts in Hydrogenation Reactions: A Patent Landscape Analysis. *Advanced Synthesis & Catalysis* **2020**, *362* (6), 1258. <https://doi.org/10.1002/adsc.201901292>.
- (43) Somorjai, G. A.; Carrazza, J. Structure Sensitivity of Catalytic Reactions. *Industrial & Engineering Chemistry Fundamentals* **1986**, *25* (1), 63-69. <https://doi.org/10.1021/i100021a009>.
- (44) Vogt, C.; Groeneveld, E.; Kamsma, G.; Nachtegaal, M.; Lu, L.; Kiely, C. J.; Berben, P. H.; Meirer, F.; Weckhuysen, B. M. Unravelling Structure Sensitivity in CO<sub>2</sub> Hydrogenation over Nickel. *Nature Catalysis* **2018**, *1*, 127-134. <https://doi.org/10.1038/s41929-017-0016-y>.
- (45) Mehdad, A.; Jentoft, R. E.; Jentoft, F. C. Highly Selective Molybdenum-Based Catalysts for Ring Hydrogenation and Contraction. *Applied Catalysis A: General* **2019**, *569*, 45–56. <https://doi.org/10.1016/J.APCATA.2018.10.012>.
- (46) Grenoble, D. C. The Chemistry and Catalysis of the Toluene Hydrodealkylation Reaction: I. The Specific Activities and Selectivities of Group VIIB and Group VIII Metals Supported on Alumina. *Journal of Catalysis* **1979**, *56* (1), 32–39. [https://doi.org/10.1016/0021-9517\(79\)90085-X](https://doi.org/10.1016/0021-9517(79)90085-X).
- (47) Musselwhite, N.; Somorjai, G. A. Investigations of Structure Sensitivity in Heterogeneous Catalysis: From Single Crystals to Monodisperse Nanoparticles. *Topics in Catalysis* **2013**, *56* (15–17), 1277-1283. <https://doi.org/10.1007/s11244-013-0150-y>.
- (48) Frauwallner, M. L.; López-Linares, F.; Lara-Romero, J.; Scott, C. E.; Ali, V.; Hernández, E.; Pereira-Almao, P. Toluene Hydrogenation at Low Temperature Using a Molybdenum Carbide Catalyst. *Applied Catalysis A: General* **2011**, *394* (1–2), 62–70. <https://doi.org/10.1016/J.APCATA.2010.12.024>.
- (49) Gates-Rector, S. ; B. T. 00-025-1047, The Powder Diffraction File: A Quality Materials Characterization Database. *Powder Diffr* **2019**, *34* (4), 352–360.
- (50) Gates-Rector, S. ; B. T. PDF.00-035-0776, The Powder Diffraction File: A Quality Materials Characterization Database. *Powder Diffr.* **2019**, *34* (4), 352–360.
- (51) Gates-Rector, S. ; B. T. PDF 00-004-0806, The Powder Diffraction File: A Quality Materials Characterization Database. *Powder Diffr* **2019**, *34* (4), 352–360.
- (52) Kurlov, A. S.; Gusev, A. I. Neutron and X-Ray Diffraction Study and Symmetry Analysis of Phase Transformations in Lower Tungsten Carbide W<sub>2</sub>C. *Physical Review B* **2007**, *76* (17), 174115. <https://doi.org/10.1103/PhysRevB.76.174115>.
- (53) Halder, N. C.; Wagner, C. N. J. Analysis of the Broadening of Powder Pattern Peaks Using Variance, Integral Breadth, and Fourier Coefficients of the Line Profile. In *Advances in X-Ray Analysis*; Springer US: Boston, MA, 1966. [https://doi.org/10.1007/978-1-4684-7633-0\\_8](https://doi.org/10.1007/978-1-4684-7633-0_8).
- (54) Safety data sheet, Methane, <https://www.airgas.com/msds/001033.pdf>, first accessed on December 03, 2020
- (55) Airgas safety data sheet, Hydrogen, <https://www.airgas.com/msds/001026.pdf>, first accessed on December 03, 2020
- (56) Compressed gases SOP, <https://ehs.umass.edu/sites/default/files/Compressed%20Gases%20SOP%20Final.pdf>, first accessed on December 04, 2020
- (57) Thermo fisher scientific safety data sheet, Toluene, <https://www.fishersci.com/store/msds?partNumber=T3244&productDescription=TOLUE>

NE+CERTIFIED+ACS+4L&vendorId=VN00033897&countryCode=US&language=en,  
first accessed on August 18, 2021